

# Phenazine 5,10-dioxide analogues as drugs against acute myeloid leukaemia.

-Preclinical documentation for lead selection

Master thesis in Pharmacy

Viola Lekve



Centre for Pharmacy and  
Department of Clinical Science

University of Bergen

May 2018



## Acknowledgements

First of all, I would like to give my sincere thanks to my supervisor Lars Herfindal for his invaluable guidance, help and support in writing this master thesis. Secondly, but no less, I would like to thank my co-supervisor Reidun Æsøy for her tireless guidance and endless patience getting me through the practical lab work. Without the pair of you, this would have been a short reading.

I would also like to thank all members of the Herfindal lab group for including me with enthusiasm and for guiding a novice researcher through the everyday challenges in the lab.

Thank you to my family for always being there for me, and a special thanks to Anna for being my flatmate for all these years, allowing our apartment to function as the headquarters of the Breakfast Club.

Last, but definitively the most, I would like to thank my friends and partners in crime throughout these five years; Tonje Sevland, Christina Lam and Erik Andreas Guldborg. Thanks for all the time, dinners, frustrations and laughs we have shared. You have made these years a true pleasure.

A special thanks to Erik, my living room-resident for the last weeks. I will miss our morning-coffee and crossword puzzle, it made the daunting task of writhing this thesis a lot easier.

I could not have done this without any of you,

*Viola Lekve*

Bergen, May 2018.



## Abstract

**Background:** Acute Myeloid Leukaemia (AML) is a form of cancer that is associated with low survival rates, and where the current treatment is impaired by low tolerance and severe side-effects. Thus, novel treatments are needed to increase the life-expectancy of AML-patients. The phenazine 5,10-dioxide compound, iodinin, has shown promising cytotoxic effects against AML cell lines in previous research. Iodinin itself has low solubility in aqueous media, and it was necessary to develop analogues with improved drug properties, which can be tested in animal models for toxicity and efficacy.

**Methods:** The cytotoxicity of the analogues IM 5, IM 20, IM 56 and IM 69 was investigated by performing viability assays on OCI-AML-3 and MOLM-13 AML cell lines and comparing the results to previously obtained results for the normal cell lines rat kidney epithelial (NRK) and cardiac myeloblast (H9c2). The generation of reactive oxygen species (ROS), by a fluorescent reporter (DCF), was also investigated for MOLM-13 and H9c2 cells. Furthermore, key factors in ROS signalling were investigated by western blot. The physiochemical properties were studied by a screening assay for membrane permeability and *in silico*-prediction of properties important for permeability and biodistribution and linked to the biological activity of the analogues.

**Results:** The analogue IM 56 showed increased cytotoxicity towards AML cell lines compared to the parent compound IM 5. It was also less toxic towards normal cell lines compared to the most frequently used AML drug, the anthracycline Daunorubicin. The difference in biological activities of the analogues is supported by their difference in membrane permeability. The analogues increase the generation of ROS in MOLM-13 cells. Except for the analogue IM 20, no such increase could be detected in H9c2 cells.

**Conclusion:** The analogue IM 56 was chosen for further drug development, due to its enhanced effect against AML cell lines relative to normal cell lines. It increases cell death in MOLM-13 cells, most likely due to generation of ROS. IM 56 is thus a promising candidate for *in vivo* pre-clinical studies.

## **Abbreviations**

AB – antibody

AML – acute myeloid leukaemia

AMPK – AMP-activated protein kinase

BSA- bovine serum albumin

CR – complete remission

Cpd. - compound

DDS – direct detect spectrophotometer

FBS- foetal bovine serum

GSH – glutathione

LUV – large unilamellar vesicles

MIR – mid-infrared region

MLV – multilamellar vesicles

NAC – N-acetyl cysteine

PAMPA – parallel artificial membrane permeability assay

PBS – phosphate buffered saline

PhF- Phenformin

PVDF – polyvinylidene difluoride

ROS – reactive oxygen species

SAS – sulfasalazine

SDS - PAGE – Sodium dodecyl sulphate polyacrylamide gel electrophoresis

SUV – small unilamellar vesicles

# Table of contents

<b>Acknowledgements</b> .....	III
<b>Abstract</b> .....	V
<b>Abbreviations</b> .....	VI
<b>1. Introduction</b> .....	9
1.1 Cancer and Acute Myeloid Leukaemia.....	9
1.1.1 Cytogenetics and cell signalling in AML.....	9
1.2 Current AML- treatment.....	12
1.3 Reactive Oxygen Species (ROS) and its relationship to cancer.....	14
1.4 Anti-cancer drug development.....	14
1.5 Analogues developed from the phenazine class compound iodinin.....	16
1.6 Aims of this master thesis.....	18
<b>2. Experimental theory</b> .....	19
2.1 Membrane permeability.....	19
2.2 HPLC.....	20
2.3 Liposomes as a tool to study drug-membrane interactions.....	21
2.4 Size exclusion chromatography.....	22
2.5 Infrared spectroscopy.....	22
2.6 Cell lines.....	23
2.7 Cell viability and EC <sub>50</sub> -values.....	23
2.8 Selected cell-active compounds used in combination with phenazine analogues.....	24
2.8.1 Sulfasalazine (SAS).....	24
2.8.2 N- acetyl cysteine (NAC).....	24
2.8.3 Phenformin (PhF).....	25
2.9 ROS detecting assay.....	26
2.10 Western blotting.....	26
<b>3. Material and methods</b> .....	28
3.1 Parallel Artificial Membrane Permeability Assay (PAMPA).....	28
3.2 HPLC-analysis.....	29
3.3 Preparation of liposomes.....	30
3.4 Compound association to liposomes.....	30
3.5 Cell lines.....	31
3.6 Assessment of cell viability by metabolic activity and nuclear morphology.....	31
3.7 Detection of reactive oxygen species in cells.....	32
3.7.1 Protocol for measuring ROS in H9c2 adherent cells.....	32

3.7.2.	Protocol for measuring ROS in MOLM-13 suspension cells.....	33
3.8.	Western Blotting.....	34
3.9.	<i>In silico</i> modelling of phenazine analogues .....	36
3.10.	Statistical analyses.....	36
<b>4.</b>	<b>Results</b> .....	<b>37</b>
4.1.	Selection of drug candidates based on in physiochemical properties and cytotoxicity towards AML cell lines.....	37
4.1.1.	The substituents determine membrane permeability of the phenazine analogues.....	37
4.1.2.	Association of analogues to liposomal membranes.....	41
4.1.3.	Investigation of the relationship between physiochemical properties, and permeability and liposome association.....	42
4.1.4.	Cytotoxic activity of analogues towards AML cell lines .....	47
4.2.	Generation of ROS in different cell lines treated with phenazine-analogues.....	51
4.2.1.	ROS-induced DCF-fluorescence is increased by analogues in MOLM-13 cells .....	51
4.2.2.	Generation of DCF-fluorescence in MOLM-13 cells is reduced by the antioxidant N-acetyl-cysteine (NAC).....	53
4.3.	Investigation of the cell signalling pathways susceptible to ROS-generation.....	56
<b>5.</b>	<b>Discussion</b> .....	<b>58</b>
<b>6.</b>	<b>Concluding remarks</b> .....	<b>67</b>
<b>7.</b>	<b>Further studies</b> .....	<b>68</b>
<b>8.</b>	<b>References</b> .....	<b>69</b>
<b>Appendix I</b> .....		<b>74</b>
Supporting Figures .....		74
<b>Appendix II</b> .....		<b>76</b>
Supporting Table 1.....		76
Supporting Table 2.....		81



# 1. Introduction

## 1.1 Cancer and Acute Myeloid Leukaemia

Cancer is a term used to describe related malignancies, which all have in common uncontrolled growth of cells. A malign cancer can utilise the blood vessels or lymphatic system to invade other parts of the body, a process called metastasis. At this stage, the cancer has often reached a life-threatening stage, and therapeutic intervention, like surgery, radiation, or chemotherapy, must be initiated (1).

Acute Myeloid Leukaemia (AML) is a form of cancer where the myeloid cells in the bone marrow are arrested at an undifferentiated state but continue proliferate. This causes accumulation of immature cells, which will take up space from the normal cells, and disturb the production of normal cells. Eventually, the AML cells will invade into the blood stream (2). The classical diagnostic feature is >20% undifferentiated myeloid blasts in a bone marrow sample (3). Numbers from the National Cancer Institute (4) show that the estimated number of new AML-cases in the US for 2017 is 21 380, and the number of estimated deaths is 10 590. The 5-year survival rate (2008-2014) was 27.4%. The median age of diagnosis is 68 years, and patients 65 years or older accounts for 57.4% of new cases, and 70.8% of deaths. The oldest patients are often those who least tolerate the current treatment, as they often have a higher rate of comorbidity factors, such as already onset heart disease, and in general have poorer ability to metabolize drugs, due to for instance slower enzymatic activity (5). The national guidelines for AML- treatment in Norway recommends a milder course of treatment for patients over the age of 65 years (6).

### 1.1.1. Cytogenetics and cell signalling in AML

AML patients represent a highly diverse group regarding cytogenetics, and there has not been identified one common denominator in the cytogenetics of these patients. There are two classification systems that subtype patients based on two different approaches (7);

- The French-American-British (FAB) classification system, which divides into categories based on which type of leukocytes the AML blasts originated from, as well as the maturation status of the blasts.

- The World Health Organisation (WHO) classification system, which is a more complex system, categorising patients emphasising alterations in their cytogenetics.

Classification based on genetic alterations makes for a better stratification of patients, as it makes use of the few common denominators that are found for certain patients, and some of these factors has shown to be significant to the prognosis for the patients. It also emphasises that there is not one mutation that is present in all AML patients.

Cytogenetic alterations include alterations affecting the factors FLT-3 ITD, p53, AMPK- and cytokine-signalling.

The FLT-3 gene encodes the fms-like tyrosine kinase 3, which is part of the receptor tyrosine kinases, and, when the receptor is activated, sends downstream signals that induce cell proliferation through STAT 5 and RAS/RAF/PI3 kinases. A mutation in the FLT-3 gene leads to constitutive activation of the receptor, and this mutation is associated with poor prognosis for the patient (8).

Mutation in the tumour suppressor gene, TP53, is also associated with poor prognosis. The gene acts as a tumour suppressor by detecting damaged DNA and signal to downstream effectors if the cell should repair its DNA or undergo apoptosis. TP53 is thus central to prevent cells with damaged DNA to proliferate and non-functional p53 (the protein TP53 encodes for) causes accumulation of mutations in the cells (9, 10).

The nucleophosmin (NPM1) gene increases the response of p53 and promotes the suppression of proliferation of damaged cells, both by direct interaction with p53, and by inhibiting a ligase that causes degradation of p53 (11). Mutation in NPM1 in the absence of FLT-3-mutation is associated with a favourable prognosis (12).

Cytokines is a class of peptide-hormones that mediates signals between cells and contribute to cell growth and proliferation. It has been shown that amongst others, IL-6 and IL-10 is upregulated in AML-patients. Elevated level of IL-6, which is a pro-inflammatory cytokine is associated with poorer prognosis, and high levels of IL-10 is associated with better prognosis (13).

AMP-activated protein kinase (AMPK) is a key regulator and sensor of the metabolic state in the cell. One of its regulators is the ATP/AMP-ratio, which will activate AMPK if the level of ATP decreases, a condition called metabolic stress (14). Activated AMPK will increase

catabolic activities like lipolysis to enhance the generation of ATP (15). As Figure 1 shows, the AMPK complex is centrally located in several pathways controlling the metabolism of a cell.

The mechanistic (or mammalian) target of rapamycin (mTOR) complex is an important kinase for protein synthesis and cell survival through the phosphorylation of the S6 kinase and 4E-binding protein 1 (4E-BP1), which when phosphorylated regulates translation of mRNA in protein synthesis. Protein kinase B (AKT) activates mTOR. The levels of AMPK and mTOR are inversely linked, as AMPK inhibits mTOR (16, 17).

The cell signalling in cancer is complex and still far from fully understood. As the factors in the cell signalling system are linked together, there are a number of potential drug targets to be identified in a cancer cell.

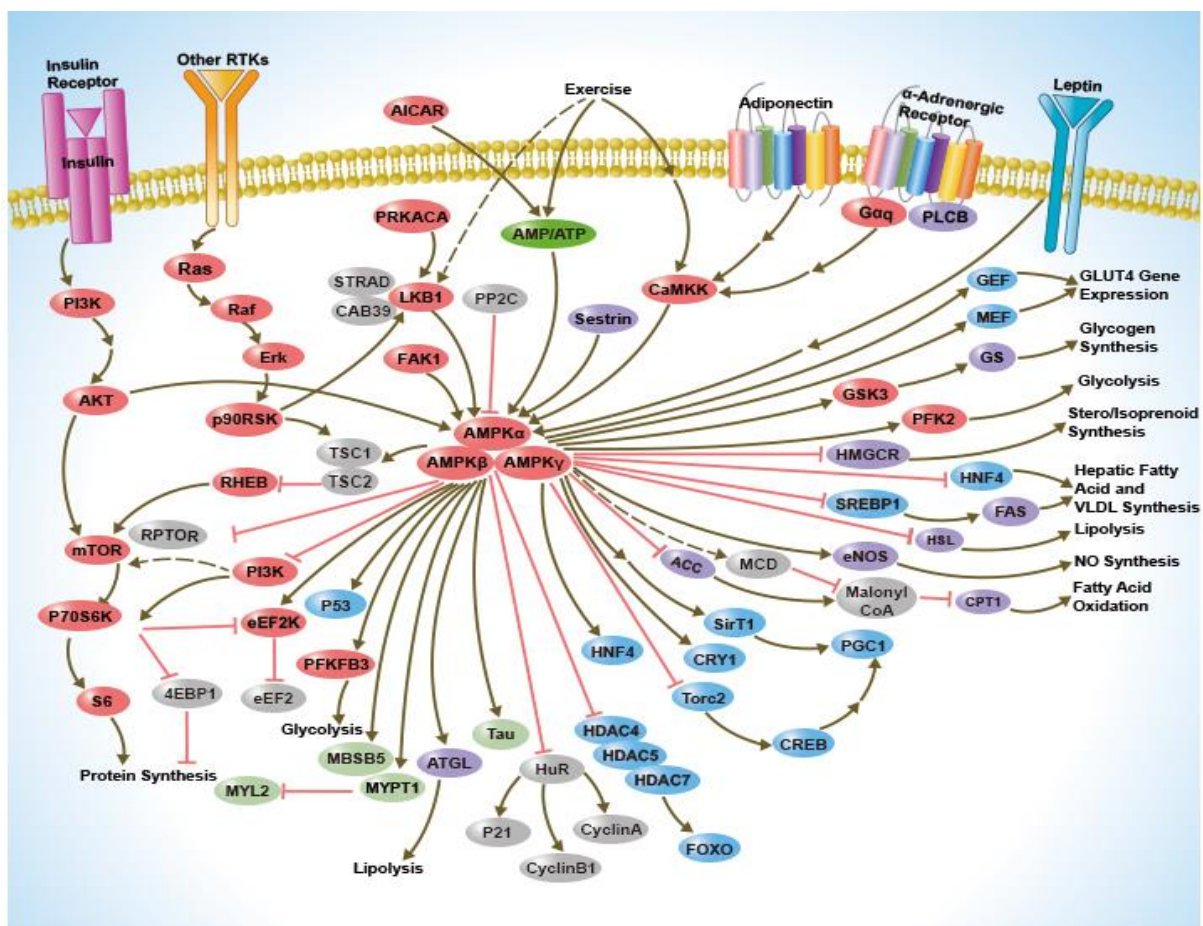


Figure 1: Schematic display of signalling pathways in a cell, focusing on AMPK-signalling. Picture downloaded from Sino Biological Inc. ([www.sinobiological.com](http://www.sinobiological.com))

## 1.2. Current AML- treatment

Since AML does not cause development of solid tumours that can be surgically removed or radiated, chemotherapy is the most common treatment, which is often harmful to normal cells and tissues. The recommended treatment for AML in Norway is summarized in the National guidelines for diagnostics, treatment and follow-up of malignant blood diseases from the Norwegian Directorate of Health. The most common course of treatment is divided into two phases, induction therapy and consolidating therapy (18). The induction phase consists of high dose chemotherapy infusions; the anthracycline daunorubicin (DNR) or idarubicin combined with the pyrimidine nucleoside analogue cytarabine. The goal of the induction therapy is to eradicate all visible signs of disease, also known as complete remission (CR) (19). CR is defined as; <5% blasts in bone marrow sample,  $>1 \times 10^9$  granulocytes/L,  $>100 \times 10^9$  blood plates/L, and absence of extramedullary manifestations.

To achieve CR it is necessary to use doses of chemotherapy which is close to the maximum tolerable dose of the patient, and in up to 5% of the cases the patient dies of complications from the chemotherapy, known as therapy related mortality (TRM) (18). These complications include granulocytopenia and thrombocytopenia; the former will also increase the risk for severe infections by opportunistic bacteria and fungi. This makes it necessary with support therapy like blood transfusions and antibiotic/antimycotic treatment. Not all patients are eligible for this intensive therapy, especially patients over 65 years of age, patients with poor general condition, and patients with other diseases that weakens their immune system. Since the group of patients over 65 years account for the majority of both new cases and deaths, and is also the group of patients that is most difficult to treat, the need of a tolerable treatment is essential.

If the patient achieves CR, the next phase of treatment is the consolidating therapy to eradicate any remaining AML cells in the blood and bone marrow, and to prevent relapse of the disease. This treatment consists of repeated cycles of chemotherapy. If there is a substantial risk of relapse, there is an option to perform allogenic stem cell transplantation. This treatment also requires pre-treatment with chemotherapy, and the TRM-rate is 15-20% in younger patients (18). The 3-year survival rate is ~50% for patients who are in CR when they receive allogenic stem cell transplantation. If the disease is still in an active state the 3-year survival is only 15% (20).

In addition to the effects the anthracyclines have on the immune system of the patients, it is commonly known that this class of compounds give a dose-dependent risk of both acute and later onset cardiomyopathy and heart failure (21). It is therefore a dire need for drugs which can be tolerated by AML patients with poor general condition, or with compromised immune system or cardiac function.

Contrary to AML, in chronic myeloid leukaemia (CML) there is identified a common denominator in the cytogenetics, where most of patients, where most of them carry a mutation in chromosome 22, which results in a constitutively active tyrosine kinase, BCR-ABL (22). An inhibitor of the BCR-ABL tyrosine kinase, imatinib (Glivec®), was developed, which led to an improved 5-year survival rate, which in 2008-2014 was 67.6% (23).

Despite the lack of a general target in AML cells, there have been some recent advances in AML therapy, and some new drugs have been approved by the FDA lately. Midostaurin is an inhibitor of the FLT-3 receptor and is used in combination with standard chemotherapy. Although contributing to a progress in AML treatment, the FLT-3 mutation is only present in ~30% of AML patients, and the effect of FLT-3 inhibitors have shown to be short-lasting (24). Vyxeos® is a fixed (5:1 molar ratio) combination of cytarabine and DNR in a liposomal formulation (25). The liposomal formulation ensures that the ratio of the drugs remain fixed compared to injecting them into the blood separately. Gemtuzumab ozogamicin (GO) is an antibody-drug conjugate targeting the CD33 antigen. It is conjugated with a calicheamicin derivative, which induces damage to the DNA of the cell (26). Not all patients are positive for the CD33 antigen, and the drug is associated with hepatotoxicity (27), which limits the benefit of the drug. Tirapazamine is a compound that induces DNA-damage through generation of radicals in hypoxic environment. It has shown favourable effects against cancer used in combination with radiation or cisplatin (28).

In conclusion, there are several treatment options for AML, but none of them represent a universal drug-therapy solution, as some of them are only specific to some cytogenetic mutations, and most of them are associated with severe side effects, and clinical trials has only demonstrated a modest increase in survival rate.

### 1.3. Reactive Oxygen Species (ROS) and its relationship to cancer

Reactive oxygen species (ROS) is the common name for molecules with unpaired electron, also known as radicals. The formation and removal of reactive oxygen species is a fine-tuned process in the cell. Endogenous factors, such as complex I in the mitochondrial respiratory chain is known to produce ROS at normal conditions, but also exogenous factors can increase the production, for instance when the body is exposed to UV- light, physical activity or redox-reactions caused by xenobiotics, resulting in what is known as oxidative stress (29). The body utilises numerous counter measures, amongst other antioxidants to remove the reactive oxygen species, see section 2.8.1 and 2.8.2 for examples.

The metabolic activity is altered in cancer cells relative to normal cells, as a part of their survival system. Cancer cells perform anaerobic glycolysis regardless of oxygen levels in the cell, known as the Warburg effect, and this is reported to increase the levels of ROS (30). The cancer cells try to counteract this by upregulation of the production of antioxidants (31).

Since high levels of ROS is known to induce cell death, several cancer treatments try to increase the ROS-production to levels beyond the point of antioxidant counteraction, or to deplete the cell of the antioxidants itself (31). One example is radiation therapy, which induces ROS-mediated DNA damage. Such treatments should preferably cause increased ROS-levels selectively in cancer cells, as increased levels of ROS can also damage normal cells and tissues. It is important that the ROS induction is high enough to surpass the stage of where cancer cells can be rescued, as low levels of ROS has shown to enhance signalling pathways linked to metastasis and tumour growth (32).

### 1.4. Anti-cancer drug development

The low survival rate of AML patients demonstrates the urgent need for new and improved treatments. Therapy with monoclonal antibodies has been described as revolutionary to the field and is important in the treatment of severe diseases like autoimmune diseases and cancers. However, the U.S. Food and Drug Administration's statistics over novel drug approvals for 2015-2017 show that small molecule compounds are still relevant in anti-cancer therapy (33). The graph shows that the main fraction of new anticancer drugs as well as other drugs has a molecular weight below 1000 Dalton (Figure 2).

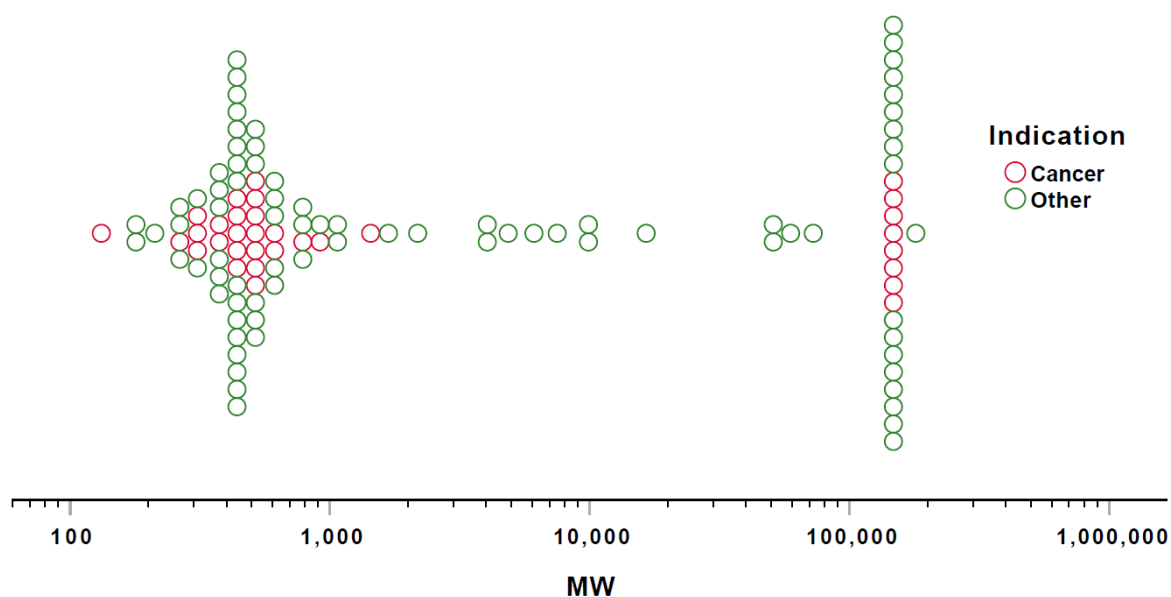


Figure 2: FDA's statistics over novel drug therapies approved in 2015-2017. The majority of both anti-cancer and other drugs have a molecular weight below 1000 Dalton. Drugs with a molecular weight ~150 000 Daltons is monoclonal antibodies.

There are several obstacles to overcome when it comes to drug development. To find a promising compound, a “hit”, it is possible to *e.g.* screen compound libraries or compounds identified from natural sources for affinity towards a known target. The hit found from the screening of compounds may not be suitable to use directly as a drug and needs to be optimized in a “hit-to-lead” process. In this process the structure of the hit might be altered to improve important properties as potency, affinity to targets, solubility, membrane permeability and stability. Many drugs have its origin in nature. A drug search based on natural sources can produce hit compounds where it is difficult to obtain substantial quantities from the natural source. It is therefore essential to be able to synthesise the natural compound. If the structure is too complex to be effectively synthesised it is possible to perform a structure-activity-relationship (SAR) study to identify which part of the structure that are essential for biological activity, and which parts that can be removed to simplify the structure and synthesis (34).

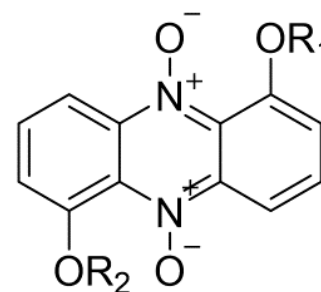
This project focus on the stage after a promising hit compound has been identified, and a method for synthesis of the drug was developed (35). The optimisation of the structure has led

to several analogues with promising properties. At this stage, further experiments must be conducted to be able to choose a lead molecule suitable for future development into a drug.

The characterisation of the analogues is important to understand or discover biological effects of the compound that cannot be predicted. One of the most important physiochemical properties of a drug is its lipophilicity (36), which will have large impact on the compounds ability to cross or interact with biological membranes. A drug's ability to interact with biological membranes will, in part, determine if and how it affects the body. Drugs that cross cell membranes, are likely to distribute in all tissues of the body. Drugs that binds to cell membranes, but do not cross, might not reach the intracellular target. Hydrophilic drugs will have poor ability to reach intracellular targets. Lipophilic drugs will bind to lipoproteins in the blood and are more likely to be distributed to adipose and liver tissue. Lipophilicity will also affect the metabolism of a drug, as lipophilic drugs get reabsorbed in the renal tubule, and are usually subjected to hepatic clearance (37).

### 1.5. Analogues developed from the phenazine class compound iodinin

The analogues used in this project are being tested for their effect as an anti-leukemic drug. The parent compounds of the analogues are iodinin and myxin, which are phenazine class compounds described to have anti-cancer and antimicrobial effect in previous literature (35, 38-40). However, iodinin has very poor solubility in aqueous solutions, which makes it difficult administer both to cells, and in animals for toxicity studies. One can therefore question the validity of previous experiments where iodinin was administered by intraperitoneal (i.p.) injection (41). Collaborators at the University of Oslo (UiO) have developed a method to synthesise iodinin (IM 5) and myxin, as well as analogues of these, and have produced several analogues with structural similarities to iodinin and myxin with improved aqueous solubility compared to the parent compounds (35, 42). Since iodinin is prepared by a new synthesis method, it will be named from the compound library identificatory (IM 5) in this master thesis. The UiO research group has synthesised close to one hundred analogues which have been tested for biological activity at the Herfindal research group at the University of Bergen (UiB). This master thesis focuses on a selected group of



R<sub>1</sub>=H, R<sub>2</sub>= H; Iodinin (IM 5)  
R<sub>1</sub>=H, R<sub>2</sub>= Me; Myxin (IM 7)

*Figure 3. Structures of iodinin (IM 5) and myxin (IM 7).*



analogues that show to be particularly promising as lead candidates based on their efficacy towards AML cells. A screening assay for permeability was performed on 42 of the analogues (see section 4.1.1), the rest of the work has been focused on the analogues denoted IM 5 (the parent compound, iodinin), IM 20, IM 56 and IM 69. See Supporting Table 1 and 2 for structures of all screened analogues.

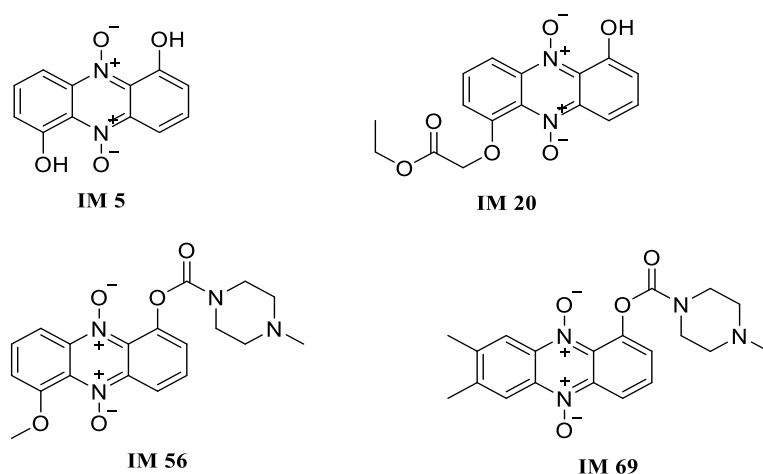


Figure 4. Structures of the analogues focused on in this project. IM 5 is the parent compound, iodinin.

The four selected analogues have the phenazine 5,10 dioxide unit as basis for the structure, but with different R<sub>1</sub> and R<sub>2</sub> substituents (Figure 3 and 4). Both R-substituents for IM 5 are hydroxy-groups, which is the basis for the alterations done in the analogues. The R<sub>1</sub> substituent of IM 20 is the same as for IM5, but the R<sub>2</sub> substituent is an ester group. The R<sub>2</sub> substituent of IM 56 is a methyl group, and the R<sub>2</sub> substituent is a 4-methyl piperazine carboxylate. The structure of IM 69 differs the most from the rest, the R<sub>1</sub> is the same as for IM 56, but the R<sub>2</sub> substituent at the C6 phenazine carbon is removed completely, and the C7 and C8 carbon is methylated.

## 1.6. Aims of this master thesis

The main aim of this master is to gather sufficient information on a selection of possible lead compounds to be able to choose one compound for further pre-clinical studies. To achieve this, I will investigate the biological activity and physiochemical properties of analogues synthesised from a parent compound.

The work can be divided into three parts.

The first part will include testing the cytotoxicity of the 3 most active analogues in OCI-AML3 cells and compare the activity to the parent compound iodinin and the anthracycline daunorubicin (DNR). Previous results had already been obtained concerning the cytotoxic effect of iodinin, myxin and analogues of these on the human AML cell line MOLM-13, and on the normal rat kidney epithelial (NRK) and cardiomyoblast (H9c2) cell lines.

The second part will include examining the physiochemical properties of the analogues in order to find if this can explain the differences in bioactivity, and to possibly be able to predict their interaction with biological membranes and their pharmacokinetic properties. Emphasis will be put on the ability to interact with membranes.

The third part will include studying the molecular mechanism of action of chosen analogues for how they induce their cytotoxic effect on MOLM-13 AML cells.

## 2. Experimental theory

### 2.1. Membrane permeability

Membrane permeability is an important feature to consider when developing a drug. For example, if the drug target is a receptor inside the cell, the effect of drug is dependent on whether it is able to cross the membrane of the cell. This mainly happens through passive diffusion or active transport across the cell membrane (43). For instance, the anthracycline daunorubicin (DNR) is proven to be a substrate for active transport over the cell membrane (44). If the cell has a defect in this transporter system, DNR will not be able to intercalate with the DNA inside the cell.

To investigate the membrane permeability of the analogues, a Parallel Artificial Membrane Permeability Assay (PAMPA) was utilised.

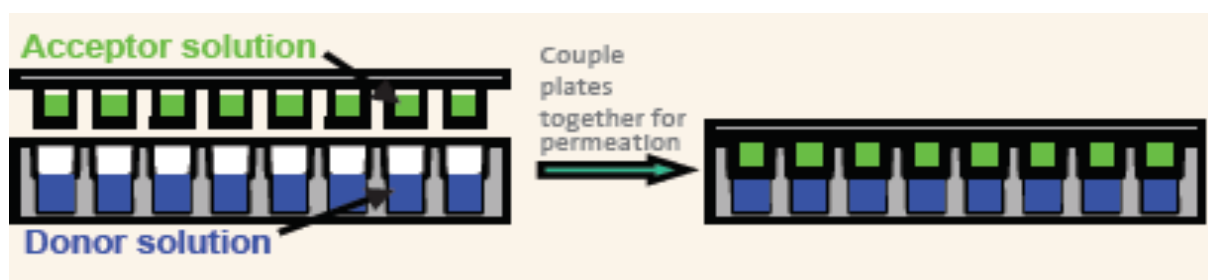


Figure 5: Plate setup for the PAMPA assay. Picture from manufacturers product catalogue, available at; [https://catalog2.corning.com/LifeSciences/en-US/Shopping/ProductDetails.aspx?productid=353015\(Lifesciences\)](https://catalog2.corning.com/LifeSciences/en-US/Shopping/ProductDetails.aspx?productid=353015(Lifesciences))

The plate system is a commercially available ready-to-use assay. It consists of one 96-well acceptor plate with a polyvinylidene fluoride (PVDF) membrane pre-coated with phospholipids as a filter in the bottom of the wells, and one 96-well donor plate, as showed in Figure 5 (45). Buffer without compounds is added to the acceptor plate, and the compounds of interest is diluted in the same buffer and added to the donor wells. Upon assembly of the plate system, the membrane is in contact with the liquid in both wells, and substances able to diffuse over the membrane will cross over to the acceptor well. The drug content in donor and acceptor wells is quantified by for instance HPLC-analysis and the ratio of the concentration of the drugs in the donor and acceptor well can be calculated as described in section 3.1. This calculation gives the value of the effective permeability,  $\log P_{\text{eff}}$ .

Bennion et al. defines the permeability from the PAMPA-assay as  $\log P_{\text{eff}} < -6.14$  as impermeable compounds,  $\log P_{\text{eff}} > -6.14 < -5.66$  as low permeability compounds,  $\log P_{\text{eff}} > -5.66 < -5.33$  as medium permeability compounds, and  $\log P_{\text{eff}} > -5.33$  as high permeability compounds (46).

Although valuable information of membrane permeability is obtained by this assay, it is important to remember that it only demonstrates the gradient-driven passive diffusion over a phospholipid membrane. It will not give information about how much substance is associated with the membrane, or if it will utilise any of the active transport systems in a cell, such as transport through an ATP-driven pump in the cell membrane.

The measured permeability found by using the PAMPA-assay,  $P_{\text{eff}}$ , was compared to  $\text{clogP}$  and  $\text{tPSA}$  values to investigate any correlation between measured permeability and important parameters for permeability calculated from the structure of the analogues.

## 2.2. HPLC

High-pressure liquid chromatography (HPLC) is a technique used to separate, identify, and quantify different analytes in a sample. In most cases, analytes are separated based on their hydrophobicity, but other physiochemical properties like charge, pH, ion strength, or size can also be used. A typical HPLC-system consists of a pump that degasses the mobile phase and maintains the desired composition and flow of mobile phase; an injector or automatic sampler which introduces the sample into the mobile phase; a column which separates the sample content; a detector (typically UV-detector) which creates a signal based on the analytes eluting from the column; and a computer with appropriate software to analyse the signal from the detector. Quantitation is done by peak integration, and based on this the amount of analyte can be calculated by comparing the values from the sample to the values from a standard curve with known concentrations (47).

When a sample is injected into the column, the different analytes will associate to the column material (stationary or solid phase) with different affinity. The difference in affinity is amongst other due to adsorption, ion exchange and partition between the components and solid phase (48). Here, a reverse phase column was used, which means that the stationary phase is nonpolar, and the mobile phase, which here are acetonitrile and MilliQ H<sub>2</sub>O, is polar.

As the gradient changes from aqueous to organic solvent, the analytes will dissociate (elute) from the column at separate time-points during the elution.

The HPLC-technique is a relatively quick and easy method, but it has some limitations. Since the affinity for the column is due to properties as adsorption and partition, it can be difficult to separate two analytes if they have similar polarity. Analytes that elute at approximately the same time and give overlapping peaks without baseline separation in the chromatogram and are difficult to quantify.

### 2.3. Liposomes as a tool to study drug-membrane interactions

Liposomes are small vesicles enclosed by a lipid membrane (49, p.14). Depending on the method of preparation, liposomes will form structures that can be divided into categories with approximate sizes (49, p.23):

- a) Multilamellar vesicles (MLVs)  
Consist of several membrane layers (lamellae), diameter usually between 100-1000 nm
- b) Large unilamellar vesicles (LUVs)  
Consist of one phospholipid bilayer, with a diameter between 100-1000 nm
- c) Small unilamellar vesicles (SUVs)  
Consist of one phospholipid bilayer, with a diameter between 25-100 nm

Here, SUVs were made by extrusion, where a uniform size distribution is obtained by extrusion through membranes (50), which yields liposomes with a size slightly smaller than the membrane pore size (49, p.53-54). The liposomes have the aqueous media on both sides of the lipid bilayer, and a compound present on the outside of the liposomes can either be repelled by the membrane, diffuse through the membrane, or associate with the membrane. After rinsing, for example by gel filtration, only the associated or encapsulated analogue remains in the liposome sample and can therefore give information about to what degree the analogue will cross or interact with a phospholipid bilayer membrane.

Three analogues were chosen to use in the liposome- model; IM 5, IM 20 and IM 23. IM 5 was chosen since this is the parent compound (Iodinine), IM 20 was chosen since it had shown

high potency in previous cell-assays. IM 23 was chosen since it had shown poor effect in previous cell-assays ( $EC_{50} = 50 \pm 0.4 \mu\text{M}$  in MOLM-13 cells), despite being almost identical to IM 20 regarding structure, and could therefore be used as a negative control.

#### 2.4. Size exclusion chromatography

Size exclusion chromatography, also called gel filtration, is a method that separates molecules or particles according to their size. A column is packed with sepharose gel beads. These beads are porous, and molecules small enough to enter the pores will be retained, whereas larger molecules will pass through the column without interfering with the beads (51). The sample is placed on top of the column and a running buffer elute the molecules through the gel. The largest molecules will elute first, and if the molecules are of uniform size they will form a band in the column and elute in the same fraction.

#### 2.5. Infrared spectroscopy

In order to determine lipid content in the liposome suspensions, infrared spectroscopy (Direct Detect ® spectrometer (DDS)) was used, which utilises infrared light absorbance at frequencies specific to the molecule structure. Mid-infrared (MIR) spectroscopy operates in the range of  $4000\text{-}400 \text{ cm}^{-1}$  ( $2.5\text{-}25\mu\text{m}$ ), and can be used to analyse samples as proteins, lipids and carbohydrates (52). For lipids, the DDS detects the absorption of infrared light in the range between  $2870$  and  $2840 \text{ cm}^{-1}$ , made by vibration of the C-H symmetric stretch in lipids (53).

A lipid sample is analysed by applying a  $2 \mu\text{L}$  drop on the sample area of a Direct Detect ® assay-free sample card. The sample area is a hydrophilic polytetrafluoroethylene membrane which is transparent in the MIR region. The machine dries the sample and applies infrared light, and measures how much of the light that gets absorbed, and calculates the lipid concentration using the Beer-Lambert-law;

$$A = \epsilon \times l \times C \qquad \text{Equation 1}$$

where  $A$  is absorbance,  $\epsilon$  is the molar absorptivity,  $l$  is the path length of the sample, and  $C$  is the concentration in the sample (52).

## 2.6. Cell lines

The MOLM -13 cell line (ACC-554), is a human AML cell line which carries an internal tandem duplication of FLT-3 (FLT-3 ITD) (54, 55). The OCI-AML-3 cell line (ACC-582) (56) is a human AML cell line without the internal tandem duplication of FLT-3. Both cell lines are suspension cells.

Since current treatment with anthracyclines is known to cause damage to the heart, the normal H9c2 rat cardiac myoblastic cell line (ATCC no: CRL-1446), was included in the study.

H9c2 is an adherent cell line, and if this cell line grows to confluency the myoblastic population will be depleted, so the cell line needs to be sub-cultured before it gets confluent (57).

Cultured cell lines represent an important model to study the effect of a desired treatment, and it can give important indications of e.g. effect and toxicity. Although important information is obtained by assays performed on cell lines, it is important to remember that the results can not directly be compared to an *in vivo* study, as a cell line is highly homogenous, and does not represent the complexity of the total system in the body. Therefore, *in vitro* studies on cell lines give the basic information needed to advance into *in vivo* studies in e.g. mice and eventually in humans.

## 2.7. Cell viability and EC<sub>50</sub>-values

To find the effective concentration (EC<sub>50</sub>) for treatments with cytotoxic compounds, which here means the concentration needed to induce 50% cell death, a WST-1 cell viability assay was performed. The EC<sub>50</sub> values for MOLM-13, H9c2, and NRK- cells (a kidney epithelial cell line from rat) has previously been determined by WST-1 and is here compared to the results from doing the same assay on OCI-AML-3 cells.

The WST-1 assay utilises the ability a metabolic active cell has to convert a tetrazolium salt, WST-1, into the reduced formazan product. This product has a distinct colour that can be detected by a spectrophotometer, measuring absorbance at 450 nm, with a reference read at 620 nm (58, 59). The tetrazolium salt is believed to be cleaved in a reduction process which is dependent on NADPH, which is formed in viable cells. This means that the more

metabolically active cells is present in the well, the more formazan is produced, and thus the colour intensity will correlate to the number of viable cells.

To confirm the results from the WST-1 assay a manual count of apoptotic/dead cells was performed. The cells were fixed in a 2 % buffered formaldehyde solution and the nuclei were visualised by adding the DNA-specific blue fluorescent dye Hoechst 33342 in the fixative (fix-solution). The dye enters the cell and binds to the adenosine-thymine rich regions of the minor groove in the DNA (60). If the cell is dead or apoptotic, its nucleus will be condensed and visible as a bright spot in the cell. In live cells the DNA is less condensed, and the nuclei appear less bright (61) . If the cells have undergone rapid and uncontrolled cell death, the apoptotic processes might not be complete, and these cells can be difficult to distinguish from normal cell nuclei. This can occur if the cells have been treated with high concentrations of a cytotoxic analogue (62).

## 2.8. Selected cell-active compounds used in combination with phenazine analogues

### 2.8.1. Sulfasalazine (SAS)

Sulfasalazine, ((E)-2-hydroxy-5-((4-(N-(pyridin-2-yl)sulfamoyl)phenyl)diazenyl)benzoic acid), is sulpha class compound, used as an anti-inflammatory drug against rheumatoid arthritis and other autoimmune diseases. It is registered in Norway under the brand name Salazopyrin EN (Pfizer) (63).

Sulfasalazine acts as an inhibitor of the  $x_c^-$  cystine/glutamate antiporter. Cystine is taken up into the cell and reduced to cysteine, which is a precursor for glutathione (GSH) (64). Glutathione acts as an antioxidant and reduces reactive oxygen species by being catalysed by the enzyme glutathione peroxidase (65). If the glutathione store in the cell is depleted by the inhibition of cystine uptake, the cell loses an important protective mechanism against ROS-induced damage and is therefore more likely to undergo apoptosis.

### 2.8.2. N- acetyl cysteine (NAC)



N- acetyl cysteine (NAC) is a thiol containing compound, which is used as a mucolytic drug, and is registered in Norway under several brand names, *e.g.* Bronkyl (Weifa) (66).

NAC is considered to be a direct scavenger of reactive oxygen species but is also a precursor of glutathione (67, 68), which means that NAC has the ability to reduce the levels of ROS in the cell. Thus, NAC acts as a protectant from ROS-induced cell death.

### 2.8.3. Phenformin (PhF)

Phenformin, (3-(diaminomethylidene)-1-ethyl-1-(2-phenylethyl)guanidine), is a compound of the drug class biguanides, which is used to treat metabolic diseases, such as diabetes. It is more potent than its related compound metformin, and associated with more severe side effects, and thus not used as an antidiabetic drug today (69). Metformin is therefore better studied, and has shown promising effects as an anti-cancer agent (70). The possible use of metformin in cancer therapy has also renewed the interest for phenformin.

Metformin is an inhibitor of complex I in the mitochondrial respiratory chain (71) and this is also shown to be true for phenformin (31, 72). The inhibition of complex I (NADH:ubiquinone oxidoreductase) prevents the coenzyme NADH from transferring electrons to complex I, and the lost energy prevents  $H^+$  from being excreted, and thus there is no influx of  $H^+$ , which drives the energy-dependent catalysis of ADP to ATP by the enzyme ATP-synthase (73, 74). Less ATP- production leads to an increase in the AMP/ATP- ratio, which in turn activate the AMP-activated protein kinase (AMPK) (75).

Since phenformin is a known activator of AMPK, it can be used as a positive control to study AMPK-phosphorylation by for instance western blotting, where it gives increased phosphorylation status compared to untreated samples.

## 2.9. ROS detecting assay

There are several fluorescent probes which can be used to measure the intracellular levels of reactive oxygen species (ROS) (76). In the present study we used 2',7'-dichlorofluorescein diacetate (DCF-DA), which is non-fluorescent in its reduced state, and permeates the cell easily. Here, cellular esterases deacetylates DCF-DA, and this deacetylated substance is oxidised by ROS to 2',7'-dichlorofluorescein (DCF). DCF emits green fluorescence, with a maximum excitation spectrum at 495 nm, and maximum emission spectrum at 529 nm (77). DCF-DA can be used in assays to measure ROS in both adherent and suspension cells.

There are some issues to consider when using the DCF-DA-assay; it cannot differentiate between the various ROS species like superoxide ( $*O_2^-$ ), hydroxyl radical ( $*OH$ ) or hydrogen peroxide ( $H_2O_2$ ), and it is not photostable (76, 78). The lack of specificity is usually not a problem if you want to measure the total amount of ROS. The low photostability influence how you should set up your assay to keep the access to light to a minimum. It is therefore important to have a satisfying control sample setup, so that it is possible to remove the background signal from both medium, untreated cells, and cells treated only with DCF-DA. If these factors cannot be controlled, there is a chance there will be large variations in the measurements.

## 2.10. Western blotting

Western blotting is a widely used method to identify specific proteins from a mixture of the total protein content in a sample. The method includes several steps; preparing a cell lysate sample, separating the proteins by electrophoresis, transferring the protein bands to a membrane, and visualisation of the protein bands by antibodies (79).

The preparation of cell lysate is done by subjecting the cells to the desired treatment, which here meant incubating cells with the analogues, rinsing the cells for excess drugs, lysing the cells to get all proteins in a mixture, and rinse the lysate from other cell components by centrifugation.

Proteins are separated using gel electrophoresis, where the mixed proteins get separated by applying an electrical force which makes the negatively charged proteins migrate through a

polyacrylamide gel (80). Smaller proteins will migrate faster than larger proteins and the proteins from the total sample are separated by their size.

The proteins from the gel is transferred (blotted) to a polyvinylidene fluorene membrane and the membrane is blocked to prevent unspecific binding of the antibodies. The membrane is incubated with primary antibodies that are specific to the protein of interest, and then re-incubated with a secondary antibody, which is specific to the species that is the source of the primary antibody (*e.g.* mouse or rabbit). The secondary antibody is often conjugated with an enzyme, which, when in contact with an appropriate substrate, will produce a detectable signal. To control that equal amounts of protein is loaded into each well of the electrophoresis gel, a loading control is used. Antibodies against  $\beta$ -actin are commonly used, as  $\beta$ -actin is a “housekeeping” protein, which is a group of proteins equally expressed in cells. This will usually give an even band for each well, provided correct loading.

Although being a widely used method, there are also some drawbacks with the method (81). It is relatively time-consuming, as the incubation for each antibody is done overnight and each step (blotting, removing of both antibodies and stripping) requires a washing cycle, here  $2 \times 5$  minutes + 15 minutes. It is also possible to get non-specific binding to proteins, or weak detection if the antibody is degraded. Correct handling of the protein samples is also important to prevent degrading of the proteins, for example by heat or proteasomes. Finally, it is relatively laborious, and not suitable for high-throughput samples.

### 3. Material and methods

#### 3.1. Parallel Artificial Membrane Permeability Assay (PAMPA)

The assay used to determine to which extent the analogues could cross membranes was the Corning® Gentest™ Pre-coated PAMPA Plate System from Corning Discovery Labware Inc (Bedford, USA). The analogue stock solutions were diluted in phosphate buffered saline (PBS) to 50 µM, and 300 µL was added to each well in the donor plate. 200 µL PBS was added to the receiver plate, the plate system assembled, and incubated for 5 hours in the dark at room temperature (21°C). After incubation, the content of each well was quantified by HPLC-analysis, and the ratio of the concentration of the analogues in the donor and acceptor well was calculated.

The effective permeability (cm/s) was calculated using Equation 2 (82):

$$P_{eff} = \frac{-\ln[1-C_A(t)/C_{eq}]}{A \times (1/V_D + 1/V_A) \times t} \quad \text{Equation 2}$$

where A is the area of the filter plate membrane (0.3 cm<sup>2</sup>), V<sub>D</sub> is the volume in the donor well (0.3 mL), V<sub>A</sub> is the volume in the acceptor well (0.2 mL), C<sub>A</sub>(t) is the concentration in the acceptor well at time t, and t is the time of incubation (18 000 s). C<sub>eq</sub> was calculated using Equation 3 (82):

$$C_{eq} = \frac{[C_D(t) \times V_D + C_A(t) \times V_A]}{(V_D + V_A)} \quad \text{Equation 3}$$

where C<sub>D</sub>(t) is the concentration in donor well at time t, and the other values are as mentioned above.

### 3.2. HPLC-analysis

The HPLC system was a Merck-Hitachi LaChrome (VWR, Westchester, USA) which consisted of Merck L-7614 pump (Merck KGaA, Darmstadt, Germany), a manual injector (Rheodyne ® model 7725i), a Kromasil 100-5 C18 150-4.6 mm column, a L-7455 diode array detector, Hitachi Interface D-7000 (Hitachi Instruments Inc., San Jose, Ca, USA), and the data processing software D-7000 HPLC System Manager (HSM), version 4.1 (Merck KGaA, Darmstadt, Germany/Hitachi Instruments Inc., San Jose, Ca, USA).

The pump was coupled to a reversed phase column (Kromasil 100-5 C18 150-4.6 mm, Akzo Nobel, Sweden), fitted with a 10 x 4.6 mm C18 guard column (Akzo Nobel, Sweden). Mobile phase A was MilliQ H<sub>2</sub>O added 0.05% trifluoroacetic acid (TFA), and mobile phase B was acetonitrile (ACN). The gradients used is shown in Table 1 and 2. Peak integration was calculated at 285 nm. The samples were injected into the column using a 250 µL syringe (Gastight ® #1725 from Hamilton Bonaduz A.G., Bonaduz, Switzerland) in a manual injector (Rheodyne ® model 7725i injector from Rheodyne (Idex Health and Science), Rohnert Park, USA).

**Table 1. Mobile phase gradient liposomes**

Time [min]	Mobile phase A (MilliQ H <sub>2</sub> O with 0.05% TFA) [%]	Mobile phase B (Acetonitrile) [%]
0.0	70	30
0.5	70	30
4.0	0	100
4.5	0	100
5.5	70	30
8.0	70	30

**Table 2. Mobile phase gradient PAMPA-samples**

Time [min]	Mobile phase A (MilliQ H <sub>2</sub> O with 0.05% TFA) [%]	Mobile phase B (Acetonitrile) [%]
0.0	90	30
0.5	90	30
4.0	0	100
4.5	0	100
5.5	90	10
9.0	90	10

### 3.3. Preparation of liposomes

Liposome solution was prepared by dissolving 24 mg 95% Lecithin (Soy) L-a-Phosphatidylcholine (Soy-95%) (Avanti Polar Lipids, Inc., Alabaster, AL, US) in chloroform (Sigma-Aldrich, St. Louis, USA). 5 mL of this solution was allowed to dry on a Laborota 4000 rotavapor, (Heidolph instruments, Germany), at room tempered water bath at 150 rpm, and pressure of 175 mbar for 45 minutes, to create a thin lipid film, followed by 2 hours at maximum vacuum pump capacity (6-7 mbar) to remove residual chloroform. The lipid film was hydrated to create LMV by adding 5 mL PBS (pH 7.4) from Sigma-Aldrich (St. Louis, USA), and shaking it on a Vortex-Genie 2, (Scientific industries Inc., New York, USA), and then on the rotavapor without vacuum for additional 25 minutes.

Small unilamellar liposomes were prepared from the liposome solution using a Mini Extruder from Avanti Polar Lipids, Inc. (Alabaster, AL, US). The liposome solution was extruded eleven times through Whatman® Nucleopore Track-Etched membrane filters with pore size 0.4 µm, 0.2µm and 0.1 µm to obtain the desired size.

Total lipid concentration in the liposome suspension was determined using a Direct Detect® spectrometer (DDS) from Merck KGaA (Darmstadt, Germany). A previously obtained standard curve (83, p.36), which gave Equation 4, was used to calculate the total lipid concentration by interpolation of a linear regression curve.

$$\text{Standard curve: } y = 0.0147x$$

$$\text{Equation 4}$$

### 3.4. Compound association to liposomes

The analogues were added to 500 µL of liposomes, at a molar ratio corresponding to 1% of total lipid concentration. The liposomes were incubated with the analogue at room temperature for 1 hour before gel filtration through a column (200 × 10 mm), (Bio-Rad, Hercules, USA), packed with Sephadex™ G50 medium from GE Health Bio-Science AB (Uppsala, Sweden) (51), using degassed PBS (pH 7.4) as running buffer. Fractions of 0.4 mL were collected using a fraction collector (Bio-Rad Model 2110, Hercules, USA).

Sample fractions were dried in a vacuum centrifuge Concentrator Plus, Eppendorf (Hamburg, Germany), and added 150  $\mu$ L of acetonitrile:milliQ H<sub>2</sub>O (30:70) to prepare the samples for HPLC- analysis. The acetonitrile was HPLC-grade from Merck KGaA (Darmstadt, Germany).

The liposome-samples were analysed using HPLC (see section 3.2), and the result was compared to the result from HPLC- analysis of a standard curve prepared for each analogue to determine the amount of analogue associated with the liposome.

### 3.5. Cell lines

The MOLM -13 and OCL-AML-3 cell lines were cultured in RPMI 1640 medium (R5886), with 50 IU/mL penicillin, 0.1 mg/mL streptomycin (P0781), 0.2 mM L-Glutamine (G7513) and 10% foetal bovine serum (FBS) added. The incubation condition was 37°C in the dark and 5% CO<sub>2</sub> in air.

The H9c2 was cultured in Dulbecco's Modified Eagle's Medium (DMEM), supplemented with 10% FBS and 0.1 mg/mL streptomycin (P0781), and incubated at the same conditions as the MOLM-13 cells. Sub-culturing the cells was done at 90% confluency. The cells were detached from the incubation flask, by washing twice with room tempered PBS and incubating with 0.33 mg/mL trypsin for 2-3 minutes at 37°C. The cells were next centrifuged at 200×G for 3 minutes and the cell pellet reseeded in fresh medium with supplements and the cells were reseeded in new culture flasks at 40-50% confluence.

All medium and supplements obtained from Sigma-Aldrich (St. Louis, MO, USA).

### 3.6. Assessment of cell viability by metabolic activity and nuclear morphology

Cell viability was assessed using WST-1 viability assay to find EC<sub>50</sub>- values for analogue treatment of OCI-AML-3 cells. These results are compared to results from other cell lines in Table 5, where the experiments have been performed by my supervisor Reidun Æsøy. The WST-1 assay was also used to study the viability of MOLM-13 cells treated with sulfasalazine (SAS) and phenformin.

Cells were incubated for 22 hours with increasing doses of analogues, daunorubicin (DNR), cell active compounds or solvent in a clear 96-well plate at a concentration of 10-20 000

cells/well and added 10  $\mu$ L WST-1 solution, which was allowed to incubate with the cells for 2 hours before measuring absorbance at 450 nm, with a reference read at 620 nm using an Infinite  $\text{\textcircled{R}}$  M200 Pro plate reader using Magellan<sup>TM</sup> software (Tecan Trading AG, Zürich, Switzerland).

Results from the WST-1 assays were confirmed by microscopic evaluation of cells fixed in 2% buffered formaldehyde (pH 7.4) containing the fluorescent DNA dye Hoechst 33342 (0.01 mg/mL) and

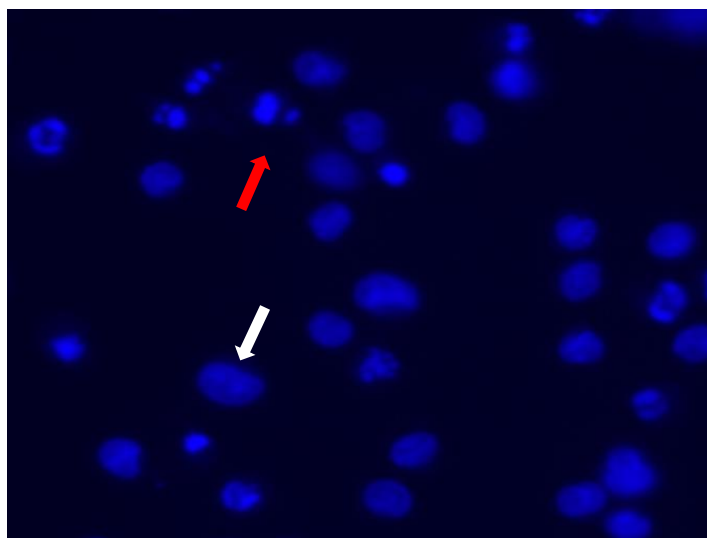


*Figure 6. Fixed cells were counted manually by microscopy to assess cell viability based on nuclear morphology. Apoptotic cell shown by red arrow. Living cell shown by white arrow.*

counting approximately 200 living and apoptotic/dead cells per well (Figure 6). The percentage of apoptosis for treated cells were adjusted relative to untreated control cells by applying Equation 5.  $D_s$  = Percent apoptosis in sample,  $D_c$  = percent apoptosis in control cells.

$$\text{Apoptosis relative to control cells} = D_s - \left( D_c \times \frac{100 - D_s}{100 - D_c} \right) \quad \text{Equation 5}$$

### 3.7. Detection of reactive oxygen species in cells

#### 3.7.1. Protocol for measuring ROS in H9c2 adherent cells

One day prior to the experiment 6000 cells were seeded per well into black 96-well plates with clear bottom and incubated at 37°C and 19%  $O_2$ .

At the day of the experiment the medium was removed from the wells, and the cells washed twice with serum-free medium. Half of the wells were incubated with 20  $\mu$ M DCF-DA in serum-free DMEM for 30 minutes in the dark, the other half with serum-free medium only.



The cells were next washed three times with PBS (37°C), and 100 µL DMEM with 10% FBS containing analogues, H<sub>2</sub>O<sub>2</sub> (positive control) or solvent was added to its respective wells and placed in the incubator. ROS generation was recorded by measuring the fluorescence at wavelengths 485 nm (excitation) and 535 nm (emission), using a Synergy H1 hybrid spectrofluorometer with the Gen5 software (version 2.00.18) from BioTek Instruments, Inc. (Bad Friedrichshall, Germany) at selected time-points.

### 3.7.2. Protocol for measuring ROS in MOLM-13 suspension cells

Two cell conditions were prepared in a 50 mL centrifuge tube; 5×10<sup>6</sup> cells were transferred to each tube, centrifuged at 200×g for 3 minutes, the supernatant decanted off, and the cells were washed once with serum-free RPMI. One tube was incubated with 20 µM DCF-DA in serum-free RPMI for 30 minutes in the dark, and one was incubated in serum-free RPMI only. The cells were washed three times in serum-free medium and resuspended in 5 mL RPMI with 10% FBS and supplements. 50 000 cells were seeded in 50 µL medium in each well of a 96 well plate, and added 50 µL medium containing FBS and supplements, as well as analogues, H<sub>2</sub>O<sub>2</sub>, or solvent to its respective wells. The cells were incubated in the dark at 37°C. ROS generation was recorded by measuring the fluorescence at wavelengths 485 nm (excitation) and 535 nm (emission) using a Synergy H1 hybrid spectrofluorometer with the Gen5 software (version 2.00.18) from BioTek Instruments, Inc. (Bad Friedrichshall, Germany) at selected time-points.

### 3.8. Western Blotting

After treatment with selected analogues or compounds, MOLM-13 cells were washed twice in isotonic saline solution by centrifugation at 1200 rpm for 5 minutes at 4°C. The cells were then lysed in 100 µL SHIE-buffer containing 10 mM Tris HCl (pH 7.5), 1 mM EDTA, 400 mM NaCl, 10% glycerol, 0.5% NP-40, 5 mM NaF, 0.5 mM sodium orthovanadate, 1 mM DTT, added cOmplete™ Mini Protease Inhibitor Cocktail from Sigma-Aldrich, Inc. (Darmstadt, Germany). The lysis was done by incubation on ice for 30 minutes before centrifugation at 13 000 rpm for 30 minutes at 4°C.

Protein concentrations were determined using the Quick Start Bradford protein assay (#500-0205) from Bio-Rad Laboratories (Hercules, USA), according to manufacturer's instructions (84, 85), using bovine serum albumin (BSA) as standard. 30 µg protein was mixed with loading buffer containing 1% SDS, 10% Glycerol, 12 mM Tris-HCl pH 6.8, 50 mM DTT and 0.1% Bromophenol Blue. The samples were heated to 100°C for 10 minutes, and then loaded on a ten percent SDS-polyacrylamide gel. The pre-labelled standard, Precision Plus Protein Standard All Blue (#1610373) from Bio-Rad Laboratories (Hercules, USA) was used as a protein ladder. The gel was run at 100 V for 90 minutes before proteins were transferred to polyvinylidene fluoride (PVDF) membranes, from GE Healthcare Life Sciences, (Buckinghamshire, UK) by electrophoresis by running the blots at 100 V for 70 minutes.

After blotting, the membranes were blocked in 5% BSA in TBS-T for 1 hour with gentle shaking, before overnight incubation at 4°C with the primary antibody. The next day the primary antibody was removed, the membranes washed in TBS-T, and incubated with the secondary antibody at 4°C overnight. See Table 3 for antibodies used.

**Table 3. Antibodies used for western blotting**

Antibody (*=secondary AB)	Molecular weight	Dilution in 5 % BSA	Source	Manufacturer
AMPK $\alpha$ (F6) #2793	62 kDa	1:1000	Mouse	Cell Signaling Technology, Inc (Danvers, USA)
Phospho-AMPK $\alpha$ (Thr172) (D4D6D) #50081	62 kDa	1:1000	Rabbit	Cell Signaling Technology, Inc (Danvers, USA)
4E-BP2 #2845	15-20 kDa	1:1000	Rabbit	Cell Signaling Technology, Inc (Danvers, USA)
Phospho-4E-BP1 (Thr37/46) (236B4) #2855	15-20 kDa	1:1000	Rabbit	Cell Signaling Technology, Inc (Danvers, USA)
Anti $\beta$ -actin	42 kDa	1:10 000	Mouse	Sigma-Aldrich, Inc (Darmstadt, Germany)
Phospho-p70 S6 Kinase (Ser371) Antibody #9208	70-85	1:1000	Rabbit	Cell Signaling Technology, Inc (Danvers, USA)
p70 S6 Kinase Antibody #9202	70-85	1:1000	Rabbit	Cell Signaling Technology, Inc (Danvers, USA)
Akt1 Antibody (B-1): sc-5298	62	1:1000	Mouse	Santa Cruz Biotechnology, Inc. (Heidelberg, Germany)
Peroxidase AffiniPure Donkey Anti-Mouse IgG (H+L) *	-	1:10 000	Donkey	Jackson ImmunoResearch Europe Ltd, (Cambridgeshire, UK)
Peroxidase AffiniPure Donkey Anti-Rabbit IgG (H+L) *	-	1:10 000	Donkey	Jackson ImmunoResearch Europe Ltd, (Cambridgeshire, UK)

Membranes were developed using SuperSignal® West Pico or West Femto Maximum Sensitivity Chemiluminescence Substrate from Thermo Fisher Scientific Inc. (Waltham, MA, USA) according to the manufacturers' protocols. The membranes were imaged by a LAS-4000 image reader from Fujifilm (Tokyo, Japan) using the ImageQuant Las4000 control software (version 1.2). After imaging the membranes were stripped using Restore™ PLUS Western Blot Stripping Buffer #46430, from Thermo Scientific Inc (Waltham, MA, USA) before re-incubation of the membranes with the antibody for the total version of the proteins.

Anti  $\beta$ -actin was used as loading control. As a control for apoptosis, before lysis, 100  $\mu$ L cell solution from each treatment condition were transferred to a 96-well plate with 2% buffered formaldehyde (pH 7.4) containing the fluorescent DNA dye Hoechst 33342 (0.01 mg/mL), and percentage of apoptosis was determined as previously described. Protein amounts was quantified from western blot pictures using the Analyze>Gel tool in ImageJ® software, version 1.51j8 (Wayne Rasband, National Institutes of Health, USA). An example of the quantification histogram of AMPK is shown in Supporting Figure 3.

### 3.9. *In silico* modelling of phenazine analogues

The clogP and tPSA values were determined by drawing the structures in ChemDraw Professional, ver. 16.0.1.4 (77) (PerkinElmer Informatics, Inc. Waltham, MA, USA), and using the “Chemical properties” window.

### 3.10. Statistical analyses

Data are presented as average and standard deviation ( $n \geq 3$ ). For  $n = 2$  the data are presented as average and the two measurements. The data was processed using Windows® Excel® 2016 MSO for Windows, ver. 16.0.8431.2046, (Microsoft corp. Washington, USA).

The Pearson correlation coefficient was determined using Windows® Excel® 2016 MSO for Windows, ver. 16.0.8431.2046, (Microsoft corp. Washington, USA). The coefficient is a number between -1 and 1 and indicates if two sets of data are related linearly. If the coefficient is -1 or 1 it indicates a perfect match, if it is 0 there is no linear relation between the data sets (86).

Analysis of variance (ANOVA) and least significant difference (LSD) post hoc tests were used to find differences in ROS generation in treated and un-treated cells. To find between-subject effects of NAC and analogues on ROS generation, a univariate analysis of variance was performed using the general linear model tool in IBM SPSS statistics for Apple, ver. 24, (IBM corp. Armonk, USA). Significance was set as  $p < 0.05$ .

## 4. Results

### 4.1. Selection of drug candidates based on in physiochemical properties and cytotoxicity towards AML cell lines

#### 4.1.1. The substituents determine membrane permeability of the phenazine analogues

As the different substituents are introduced, the new compounds will have altered chemical properties compared to the parent compound. This will again influence how the compounds behave in *in vitro* cell experiments, and eventually also in the blood. One chemical property that determines both cytotoxicity and biodistribution of drugs is the ability to diffuse through membranes. To assess to which extent the phenazine-analogues could passively cross membranes, the parallel artificial membrane permeability assay (PAMPA) was used. The effective permeability  $P_{\text{eff}}$ , was calculated by applying Eq. 2 and 3 in section 3.1 on the ratio between the donor and acceptor well. The calculation for each analogue gave the results presented in Figure 7. The analysis of 42 analogues show that 32 analogues can be classified as having high membrane permeability, two had intermediate permeability, three had low permeability, and five analogues were impermeable. The parent compounds iodinin and myxine (IM 5 and IM 7 respectively) were classified as low (IM 5) and high (IM 7) permeability compounds. For comparison, the N-oxide containing compound tirapazamine (TPZ) and the AML drug daunorubicin (DNR) was also tested. TPZ had low membrane permeability, whereas DNR was found to be impermeable. IM 56 was classified as a low permeability compound, and IM 20 and IM 69 was classified as high permeability compounds.

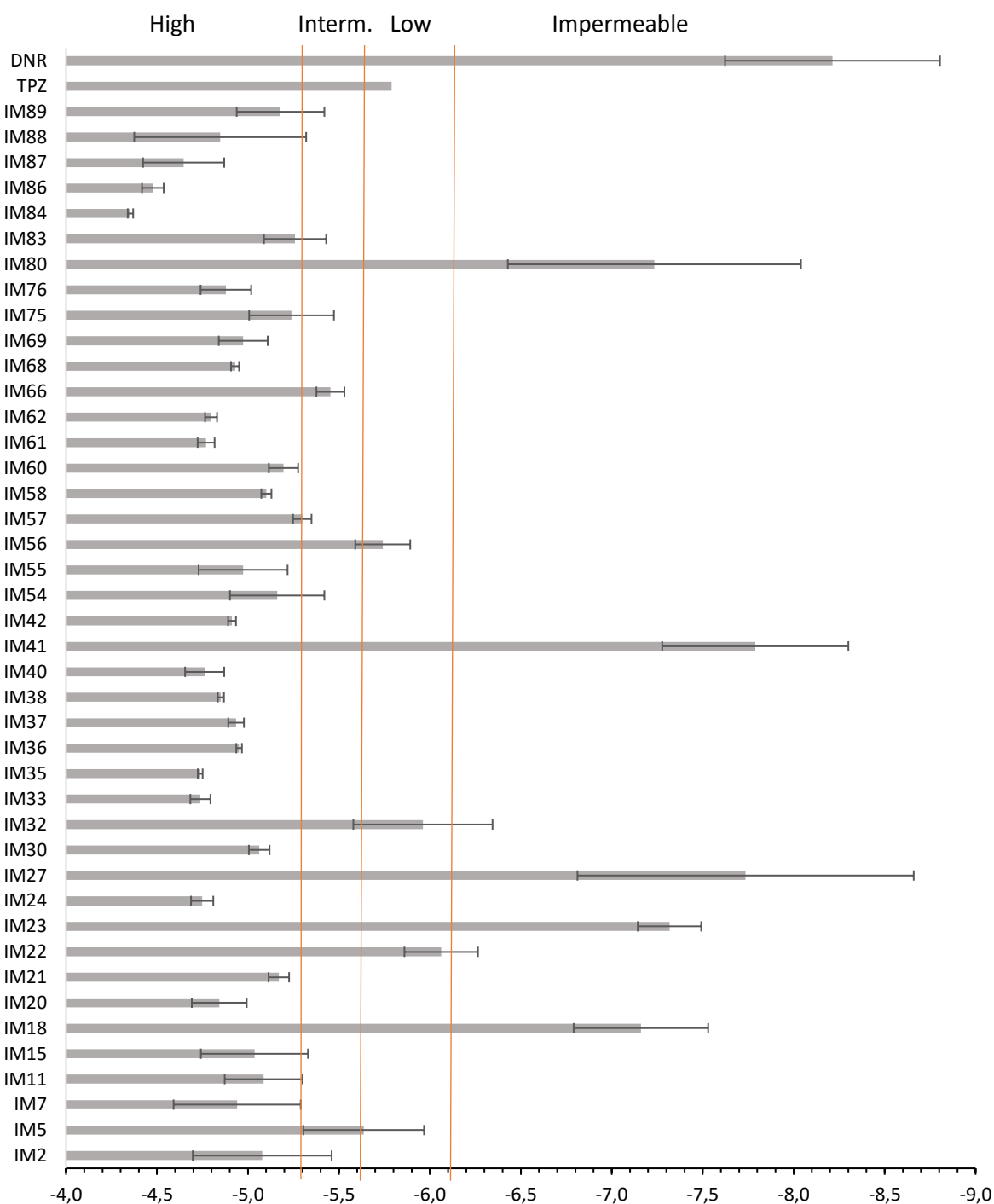
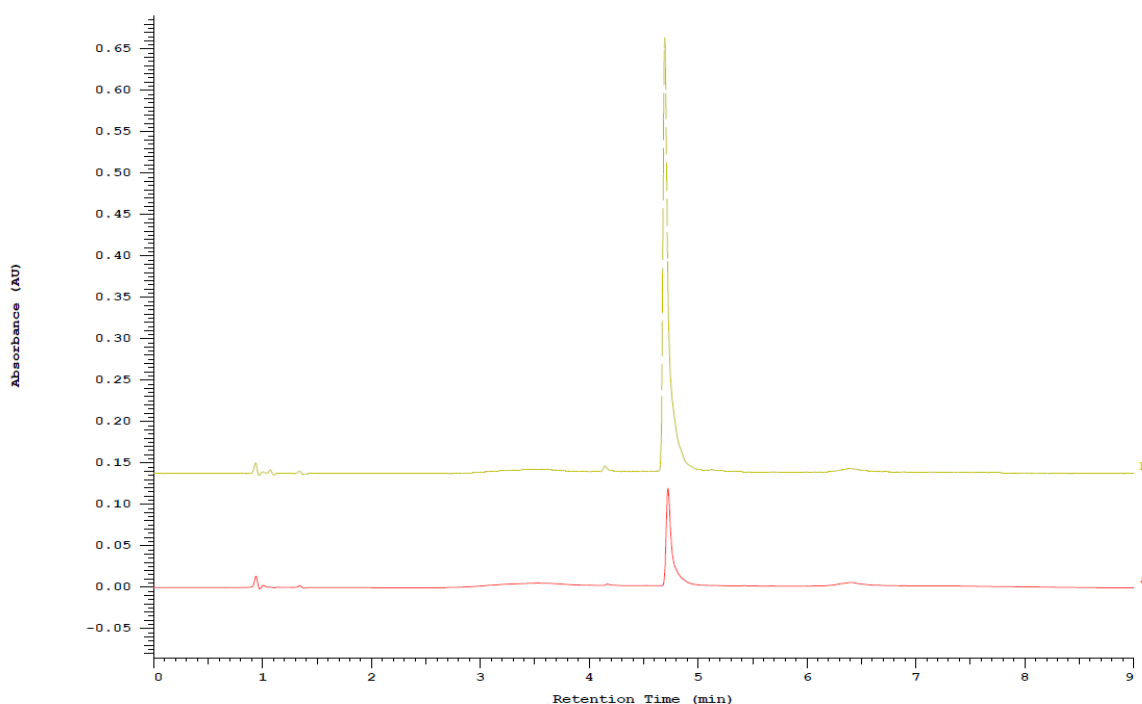


Figure 7. The diverse analogues show differences in permeability. The effective permeability  $P_{\text{eff}}$  was calculated using results from the HPLC-analysis and applying them in Equation 2 and 3, as described in section 3.1 and 3.2. The PAMPA assay defines drug permeability as high when  $\log P_{\text{eff}} > -5.33$ , intermediate as  $\log P_{\text{eff}} > -5.66 < -5.33$ , low as  $\log P_{\text{eff}} > -6.14 < -5.66$  and impermeable if  $\log P_{\text{eff}} < -6.14$ .  $n=2$  for IM 21, IM 24, IM 30, IM 33, IM 35, IM 36, IM 37, IM 38, IM 41, IM 42, IM 54, IM 57, IM 58, IM 60, IM 61, IM 62, IM 66, IM 68, IM 75, IM 76, IM 84, IM 86, IM 87, tirapazamine (TPZ) and daunorubicin (DNR).  $n= 3-9$  for IM 2, IM 5, IM 7, IM 11, IM 15, IM 18, IM20, IM 22, IM 23, IM 27, IM 32, IM 40, IM 55, IM 56, IM 69, IM 80, IM 83, IM 88 and IM 89. Whiskers show stdev. for analogues with  $n > 2$ , and highest and lowest values for analogues with  $n=2$ .

During the HPLC-analysis of the PAMPA samples most analogues eluted as a single, distinct peak as shown for IM 20 (Figure 8). Also, in most cases, the peak of the donor well was larger than that of the acceptor well, as shown by the multi-display of the chromatograms for donor and acceptor well (Figure 8), which indicates that the concentration of the compound is higher in the donor well than the acceptor well. The higher the difference, the less compound has been diffusing over the membrane.



*Figure 8. Multi-display of the HPLC-chromatograms obtained at wavelength 285 nm for donor (yellow) and acceptor (red) well of IM 20. The analogue eluted as a distinct peak with a retention time of 3.95 minutes for both donor and acceptor, but smaller amounts of the analogue is present in the acceptor well.*

In some cases, it was noticed that the analogue eluted in more than one peak, for instance the analogue IM 23. Structure for IM 23 is shown in Supporting Table 1. As presented by the multi-display of the chromatograms of the donor and acceptor well in Figure 9, the donor well (yellow line) showed several peaks with a retention time between 3.9 and 7 minutes, and it was not possible to separate the peaks. This was in contrast to the chromatogram obtained from the stock solution, which showed one distinct peak similar to IM 20 (not shown). The chromatogram from acceptor well for IM 23 (Figure 9, red line) shows that small amounts of the analogue cross the phospholipid membrane. The ratio for AUC for all peaks in the donor well compared to the acceptor well was 940:1.

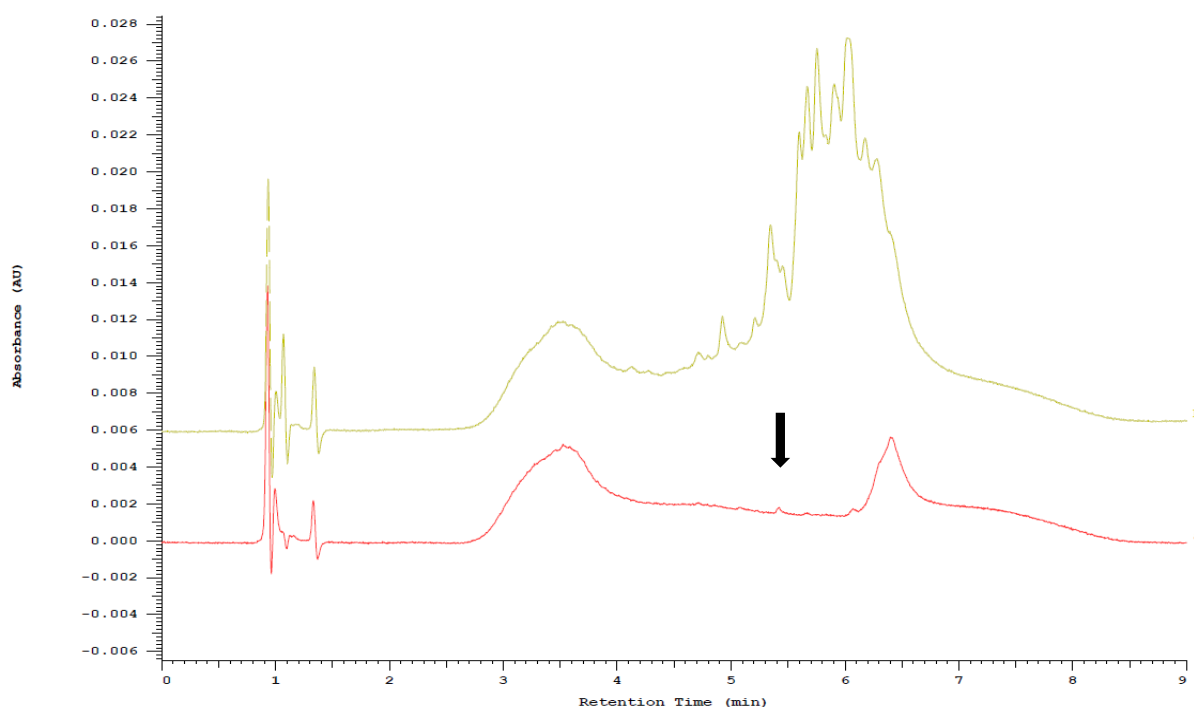


*Figure 9. Multi-display of the HPLC-chromatograms obtained at wavelength 285 nm for donor (yellow) and acceptor (red) well of IM 23. The analogue eluted as several peaks with a retention time of approximately 3.90-7.00 minutes for the analysis of the donor well. Little of the analogue crosses the phospholipid membrane, the peak identified as an analogue is marked by arrow. The peak at approx. 6.5 minutes is generated by the gradient.*



#### 4.1.2. Association of analogues to liposomal membranes

Although the analogues' ability to cross membranes is predicted in the PAMPA assay, this assay cannot determine if a compound interacts with the membrane without crossing it. Interactions with lipid membranes can also predict the means of transport in the blood (e.g. lipoproteins), or accumulation in fat tissues or organs with high lipid content, such as the brain. Liposomes were prepared to investigate if selected analogues could associate with the liposome membrane. This laborious method is much more time-consuming than the high-throughput PAMPA assay, and only three analogues were tested on the liposome model for lipid association.

In order to quantify the amount of analogue associated with the liposomes, a standard curve of each analogue was prepared using HPLC (Figure 10). These gave linear trendlines with  $R^2$ -values  $>0.995$  for all three analogues, which was considered a good fit to use to calculate amount of analogue in the liposome samples. IM 5 eluted at approximately 4.6 minutes, IM 20 eluted at approximately 4.0 minutes, and IM 23 eluted at approximately 4.3 minutes. All analogues eluted as a single, sharp peak, similar to the chromatogram shown for IM 20 (Figure 8).

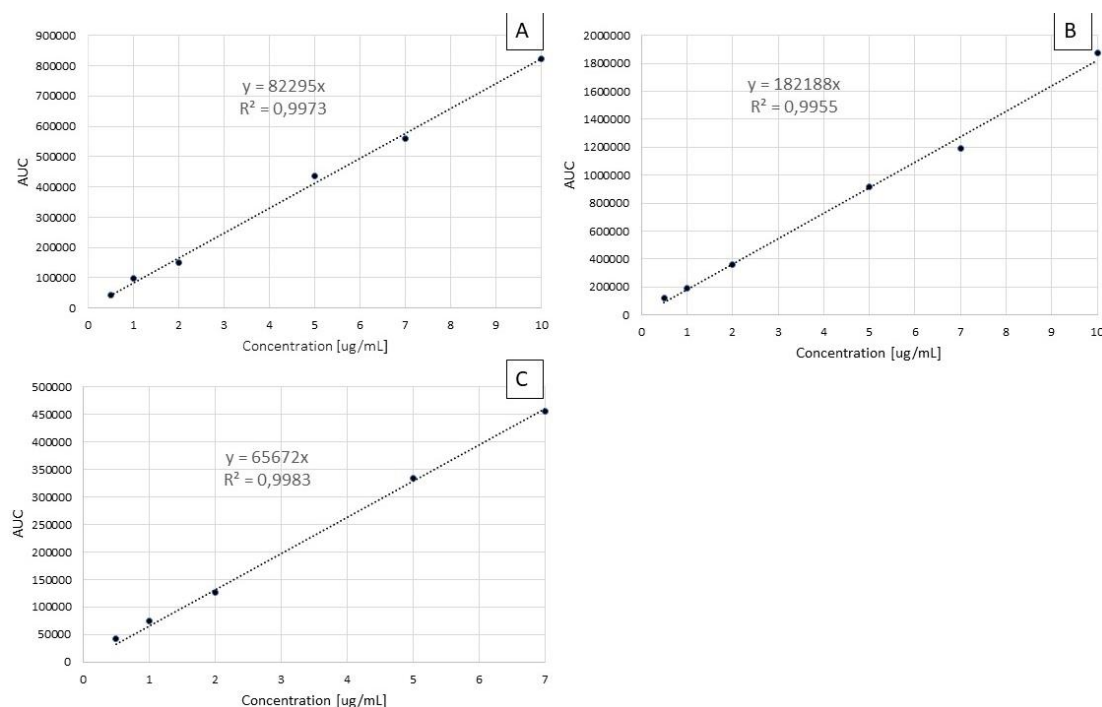


Figure 10. Standard curves were prepared to calculate the concentration of analogue in the liposome samples. Standard curves for IM 5 (C), IM 20 (B) and IM 23 (A) were prepared by diluting stock samples in MilliQ H<sub>2</sub>O and acetonitrile. The samples were analysed using the same method as the liposome samples (method in section 3.2). The  $R^2$ -value is  $>0.995$ , which is a good fit.

In the liposomes incubated with IM 5, the analogue could be observed by HPLC-analysis in fraction 14-20 from the gel filtration. It eluted at 4.60 minutes, and the calculated liposome association for the combined fractions was 17.2%.

In the liposomes incubated with IM 20, the analogue could be observed by HPLC-analysis in fraction 12-23 from the gel filtration. It eluted with two peaks, one at 3.99 minutes, and the other at 4.22 minutes, and the calculated liposome association for the combined fractions was 3.8%.

In the liposomes incubated with IM 23, the analogue could be observed by HPLC-analysis in fraction 14-21 from the gel filtration. As with the PAMPA assay, IM 23 eluted as several peaks with retention times between 3.84 – 5.89 minutes, and the calculated liposome association for the combined peaks for the combined liposome fractions was 7.2%.

The result from all three analogues is summarised in Table 4.

**Table 4. Retention time and liposome association**

Analogue	Approx. retention time [min]	Liposome association [%]
IM 5	4.60	17.2
IM 20	3.99	3.8
IM 23	3.84-5.89	7.2

#### 4.1.3. Investigation of the relationship between physiochemical properties, and permeability and liposome association

Since the analogues are derivatives of the same parent compound, and thus have structural similarities, linear regression was used to investigate if there could be found any relationship between physiochemical properties, permeability and liposome association of the analogues.

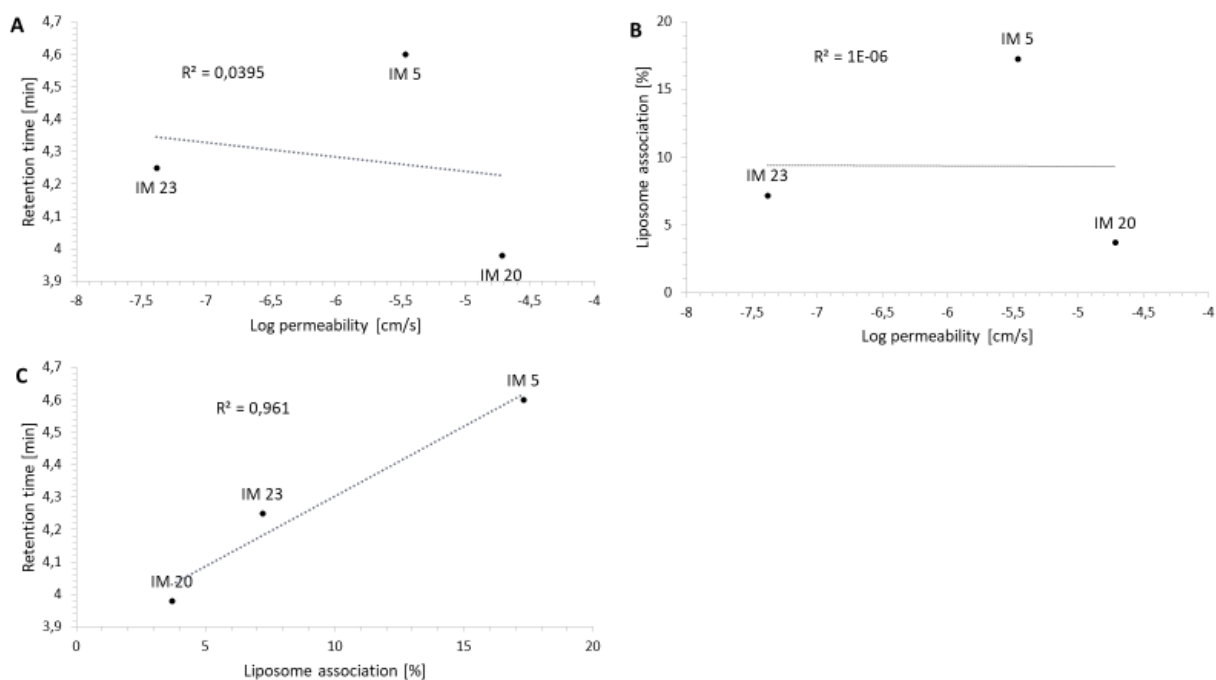


Figure 11. Analysis of liposome samples by HPLC, see section 3.2 for method. No correlation was found between retention time and permeability (A), or between liposome association and permeability (B). There was found a strong relationship between retention time and liposome association, as shown by the  $R^2$ -value = 0.962

For the liposome samples there was not found any correlation between retention time in the HPLC-column and effective permeability calculated from the PAMPA assay, as shown in Figure 11A. There was not found any correlation between liposome association and effective permeability, as shown in Figure 11B.

There was however, a strong relationship between retention time of each analogue obtained from the standard curve and liposome association (Figure 11C), with an  $R^2$ -value of 0.962, and a Pearson-correlation coefficient of 0.982.

The effective permeability ( $\log P_{\text{eff}}$ ) was calculated from the PAMPA-assay for 42 analogues as described in section 3.1, and the calculated  $\log P$  (clogP) was obtained by *in silico*-modelling in ChemDraw as described in section 3.9. Comparing clogP and  $\log P_{\text{eff}}$  showed that there was no correlation between the two properties (Pearson-correlation coefficient = -0.0191).

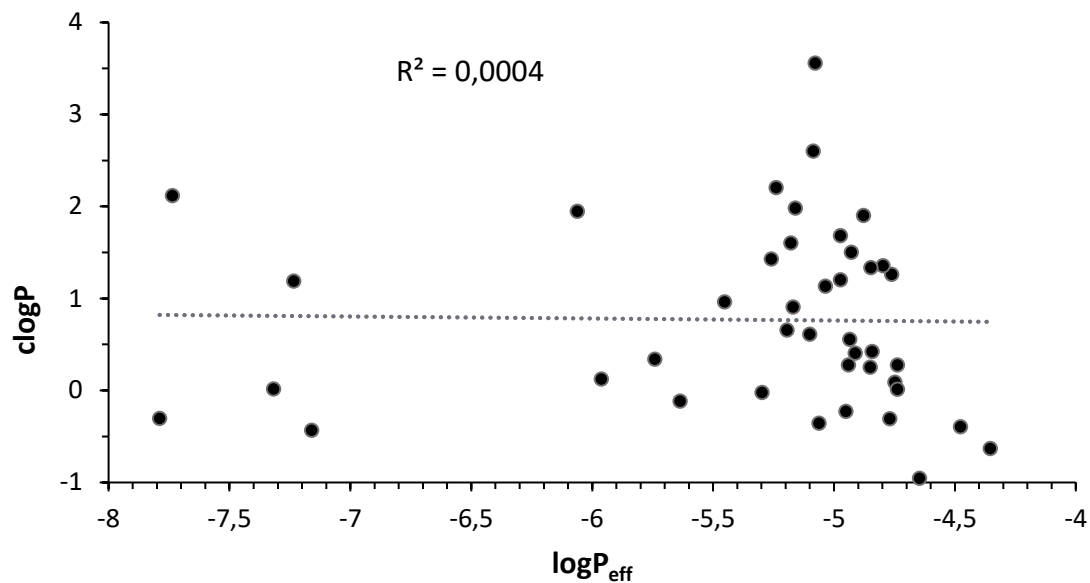


Figure 12. Scatter plot of calculated log P (clogP) values obtained by *in silico* modelling using ChemDraw as described in section 3.9, and effective permeability ( $\log P_{\text{eff}}$ ) values calculated from the PAMPA assay showed no correlation.

The effective permeability was also compared to the total polar surface area (tPSA) obtained by the same method as clogP. No correlation was found (Pearson-correlation coefficient = -0.3034).

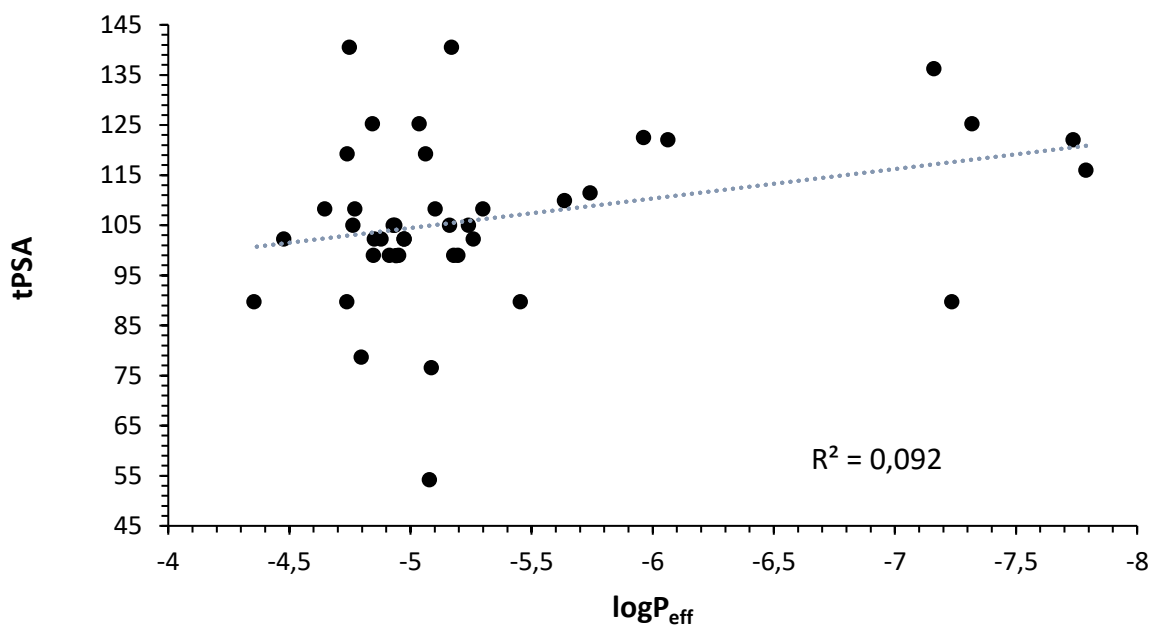


Figure 13. Scatter plot comparing the effective permeability ( $\log P_{\text{eff}}$ ) calculated from the PAMPA assay and total Polar Surface Area (tPSA) obtained by *in silico* modelling using ChemDraw as described in section 3.9 showed no correlation.

Two of the analogues studied in this project (IM 56 and IM 69) contain a piperazine substituent (Figure 4). To investigate if this substituent had any effect on the correlation between the effective permeability and calculated logP, all analogues containing the piperazine- substituent was compared, using the same methods as mentioned previously. No correlation was found (Pearson-correlation coefficient = 0.1077).

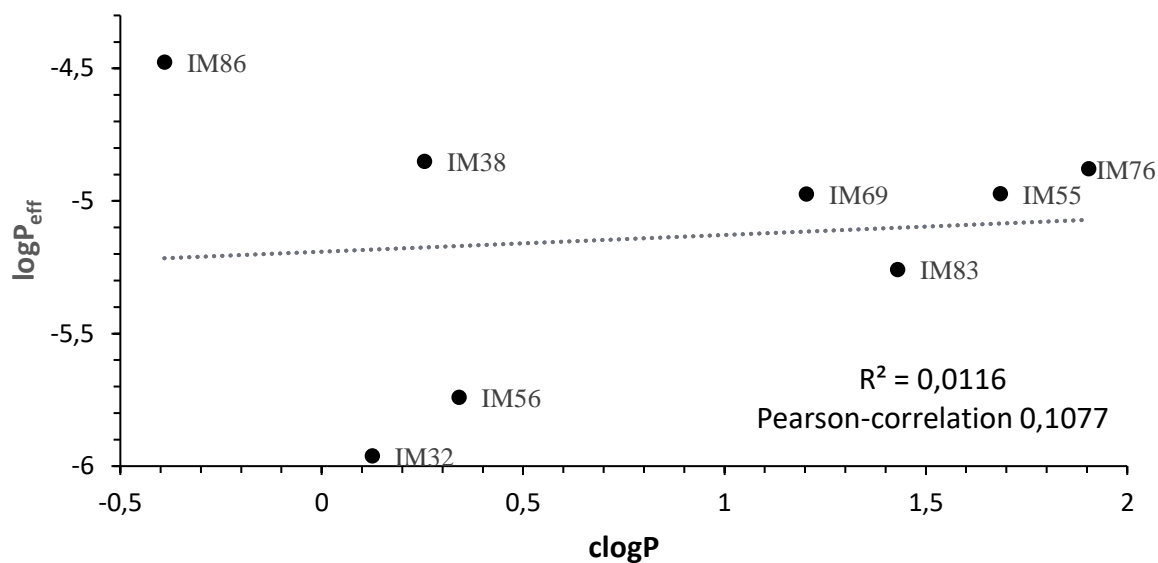


Figure 14. Scatter plot of calculated log P (clogP) values obtained by *in silico* modelling using ChemDraw as described in section 3.9), and effective permeability (logP<sub>eff</sub>) values calculated from the PAMPA assay showed no correlation.

The piperazine-containing analogues were also investigated for a relationship between effective permeability and total polar surface area. The regression analysis performed showed an intermediate relationship between the two properties (Pearson-correlation coefficient = -0.8669).

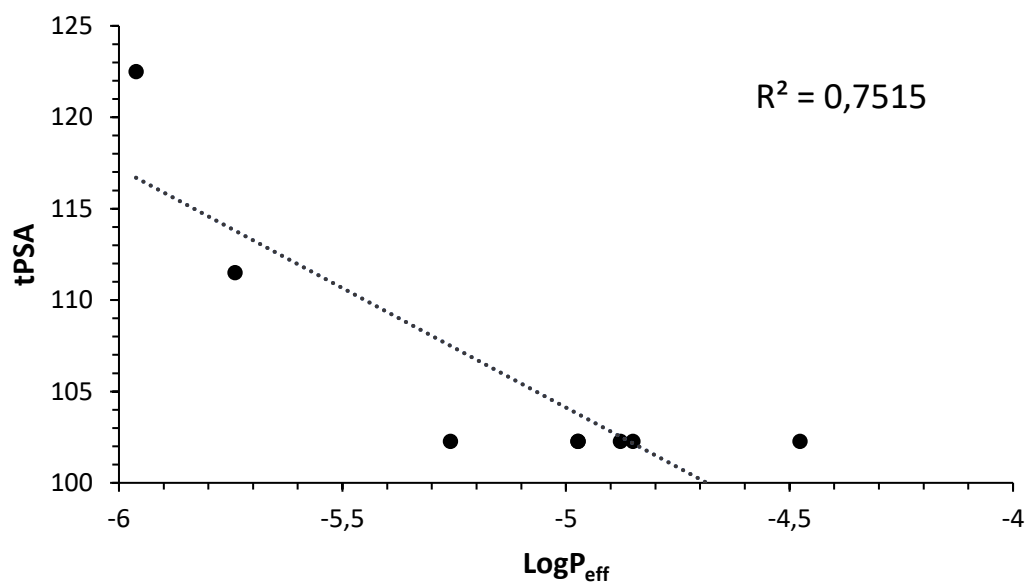


Figure 15. Scatter plot comparing effective permeability ( $\log P_{\text{eff}}$ ) calculated from the PAMPA assay and total Polar Surface Area (tPSA) obtained by *in silico* modelling using ChemDraw as described in section 3.9 for analogues containing the piperazine unit showed a linear correlation.

#### 4.1.4. Cytotoxic activity of analogues towards AML cell lines

The WST-1 assay, which measures metabolic activity, was used to assess the toxicity of the analogues and calculate their  $EC_{50}$ -value for the different cell lines. It showed that DNR was more potent than the analogues in both hypoxic and normoxic conditions, and that it was more effective in hypoxic conditions than normoxic ( $EC_{50}$ -value  $0.10 \pm 0.08$  vs  $0.24 \pm 0.00$ ). The iodinin-analogues also had lower  $EC_{50}$ -values in hypoxic conditions for OCI-AML-3 cells, except from IM 5, but the deviation from the mean was large for the hypoxic  $EC_{50}$ -value of IM 5 ( $2.64 \pm 0.33$  normox. vs  $3.79 \pm 1.07$  hypox.). The results are displayed in Figures 17 and 18 and compared to other cell lines in Table 5.

As presented in Figure 16, the result for both normoxic (A) and hypoxic (B) conditions showed a correlation between the WST-1 signal and the manual apoptosis count, with a  $R^2$ -value of 0.9077 for normoxia, and 0.7132 for hypoxia.

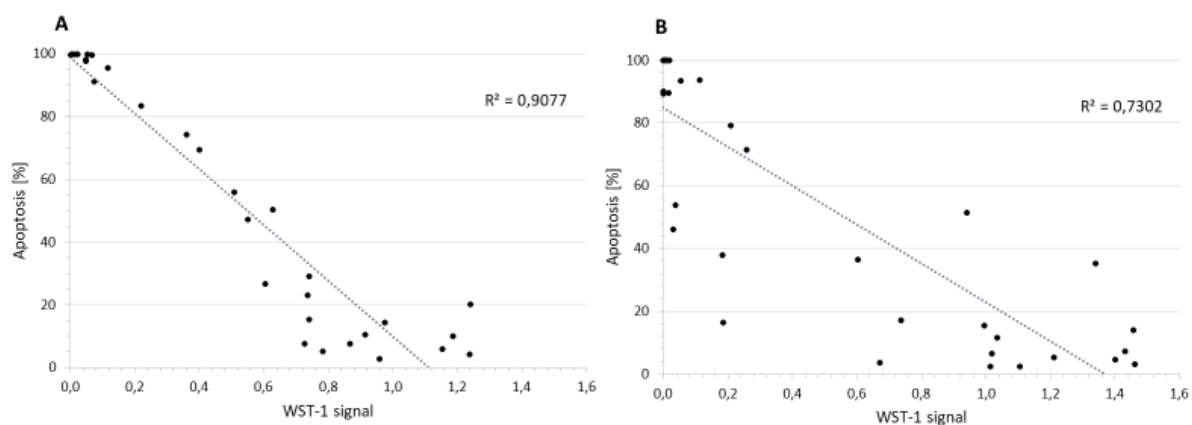


Figure 16. Scatter-plot of WST-1 signal and percent apoptosis for all treatments with analogues, as described in Figure 17 and 18, show a linear correlation between the WST-1 signal and apoptosis count. (A) Result for normoxic conditions. (B) Result for hypoxic conditions.

The individual presentation of the WST-1 signal and percent apoptosis for each analogue is shown in Figure 17 (normoxia) and Figure 18 (hypoxia).

For the normoxia treatment the Pearson-correlation coefficient showed a good fit for all drugs, with values below -0.940 for all analogues except from IM 5, which had a correlation coefficient of -0.713, regarded as an acceptable fit.

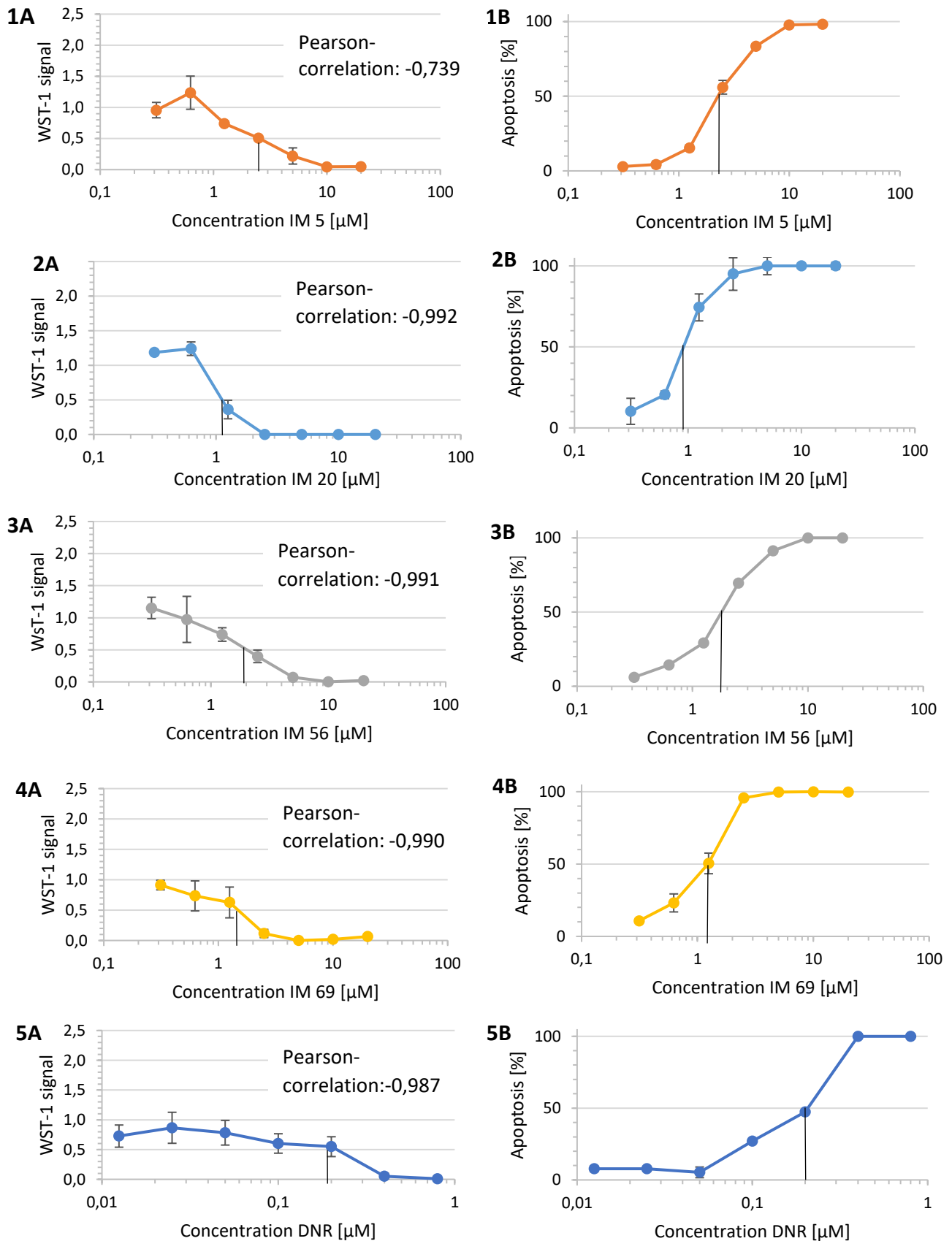


Figure 2. WST-1 viability assay performed on OCI-AML-3 cells in normoxic (19%  $\text{O}_2$ ) conditions as described in section 3.6. WST-1 results (1A-5A) are shown as WST-1 signal of treated cells relative to that of untreated control cells and compared to percent apoptosis (1B-5B) for each analogue and DNR. Pearson-correlation coefficient comparing the data sets is displayed on the WST-1 signal graph. Note the difference in the x-axis for DNR (5A and 5B).  $n=2$  and whiskers represent highest and lowest reading.



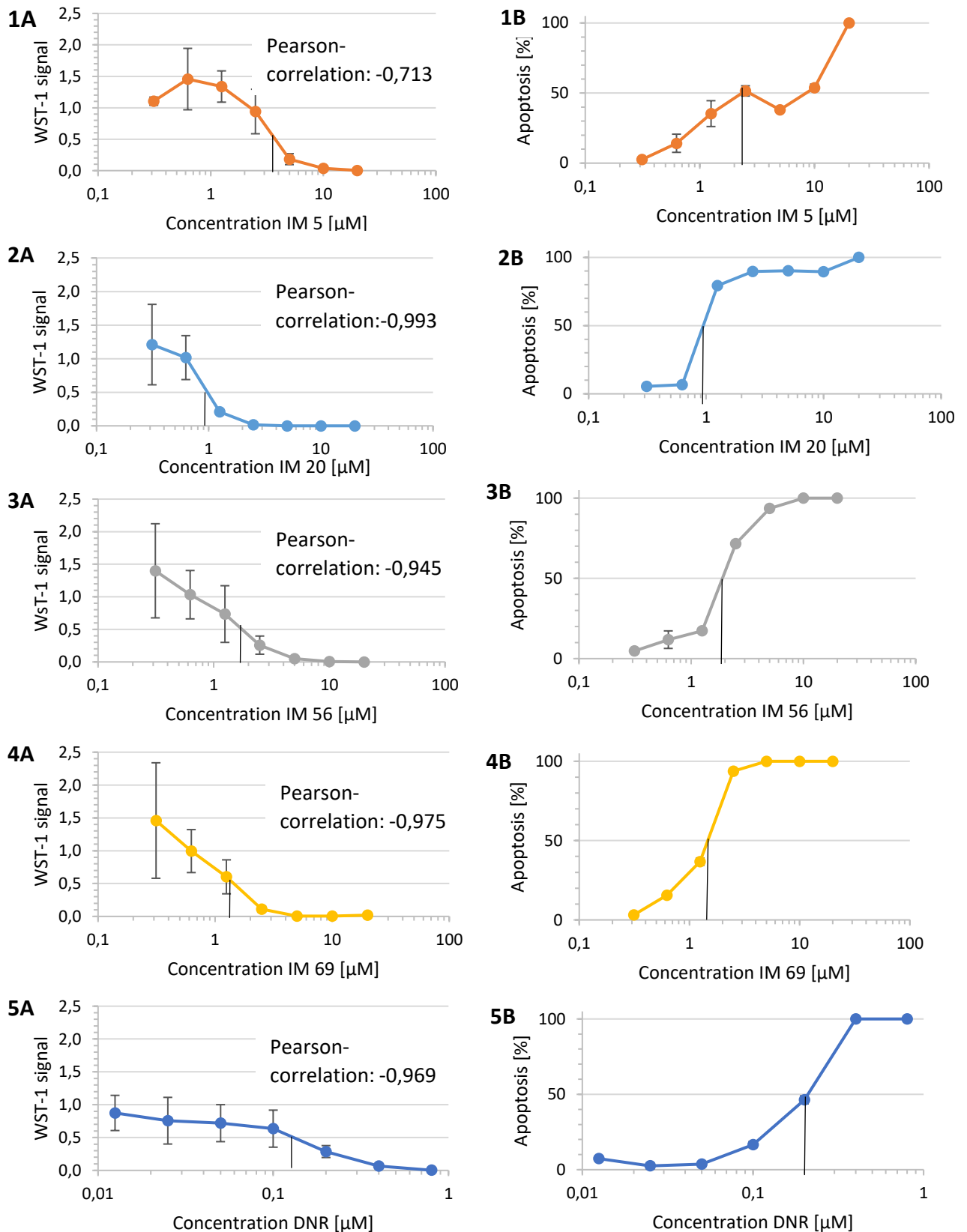


Figure 38. WST-1 viability assay performed on OCI-AML-3 cells in hypoxic (1.5%  $\text{O}_2$ ) conditions as described in section 3.6. WST-1 results (1A-5A) are shown as WST-1 signal of treated cells relative to that of untreated control cells and compared to percent apoptosis (1B-5B) for each analogue and DNR. Pearson-correlation coefficient comparing the data sets is displayed on the WST-1 signal graph. Note the difference in the x-axis for DNR (5A and 5B).  $n=2$  and whiskers represent highest and lowest reading.

The summarised presentation comparing the EC<sub>50</sub>-values for each analogue in different cell lines is shown in Table 5. It shows that the analogues are more potent (have lower EC<sub>50</sub>-values) in hypoxic environment than in normoxic environment in the AML-cell lines MOLM-13 and OCI-AML-3. In the NRK cell line, which represents normal kidney epithelia, the analogues are less potent in hypoxic conditions (for IM 5 the value is >50 for both conditions).

The results also show that the analogues are less potent against NRK and H9c2 cells than AML cell lines. For DNR the ratio for EC<sub>50</sub>-values for H9c2 against values for OCI-AML-3 in normoxic conditions is 4.2, for IM 5 the ratio is >18.9, for IM 20 the ratio is 12.2, for IM 56 the ratio is 13.4, and for IM 69 the ratio is 7.3.

Table 5. EC<sub>50</sub>-values [ $\mu$ M] ( $\pm$ SEM) of iodinin-analogues in human AML cell lines (MOLM-13 and OCI-AML-3) compared to rat kidney epithelial (NRK)- and cardiac myeloblast (H9c2) cell lines <sup>a</sup>.

Cpd.	MOLM-13**		OCI-AML-3		NRK**		H9c2**
	Normoxia	Hypoxia	Normoxia	Hypoxia	Normoxia	Hypoxia	Normox.
<b>IM 5</b>	2.00 $\pm$ 0.07	0.79 $\pm$ 0.10	2.64 $\pm$ 0.33	3.79 $\pm$ 1.07	> 50	>50	>50
<b>IM 20</b>	0.57 $\pm$ 0.06	0.49 $\pm$ 0.12	1.23 $\pm$ 0.03	0.92 $\pm$ 0.28	11.0 $\pm$ 1.6	18.0 $\pm$ 1.5	15 $\pm$ 0.9
<b>IM 56</b>	1.00 $\pm$ 0.06	0.98 $\pm$ 0.08	1.94 $\pm$ 0.52	1.60 $\pm$ 0.86	26.0 $\pm$ 2.1	39.0 $\pm$ 4.2	26 $\pm$ 0.9
<b>IM 69</b>	0.63 $\pm$ 0.05	0.54 $\pm$ 0.06	1.28 $\pm$ 0.57	1.27 $\pm$ 0.54	11.0 $\pm$ 11.5	13.0 $\pm$ 0.7	9.4 $\pm$ 0.55
<b>DNR</b>			0.24 $\pm$ 0.00	0.10 $\pm$ 0.08			~1*

a. The cells were treated with various doses of the analogues IM 5, IM 20, IM 56 and IM 69, or Daunorubicin (DNR) for 24 hours, either in normoxia (19% O<sub>2</sub>) or hypoxia (1.5% O<sub>2</sub>), before cell viability was assessed by WST-1. The data are based on regression analyses of 2 to 4 experiments and are adjusted relative to untreated control cells in each experiment using Equation 5.

\* The EC<sub>50</sub>-value of DNR in H9c2 cells is estimated from Figure 5 in Myhren et al (2013) (87).

\*\* Results previously obtained by Reidun Æsøy.

## 4.2. Generation of ROS in different cell lines treated with phenazine-analogues

### 4.2.1. ROS-induced DCF-fluorescence is increased by analogues in MOLM-13 cells

The generation of DCF-fluorescence, which is used as an indicator of ROS-generation, increased in MOLM-13 cells treated with the analogues IM 5, IM 69, IM 56 and IM 20 (Figure 19). The increase appeared dose-dependent for IM 69, IM 56 and IM 20. Treatment with DNR did not show an increase in ROS-generation in MOLM-13 cells. IM 20 gave the strongest DCF-fluorescence measurements of all concentrations, where 9  $\mu\text{M}$  gave an increase of about three times what was observed in the untreated cells (Figure 19 A and B).

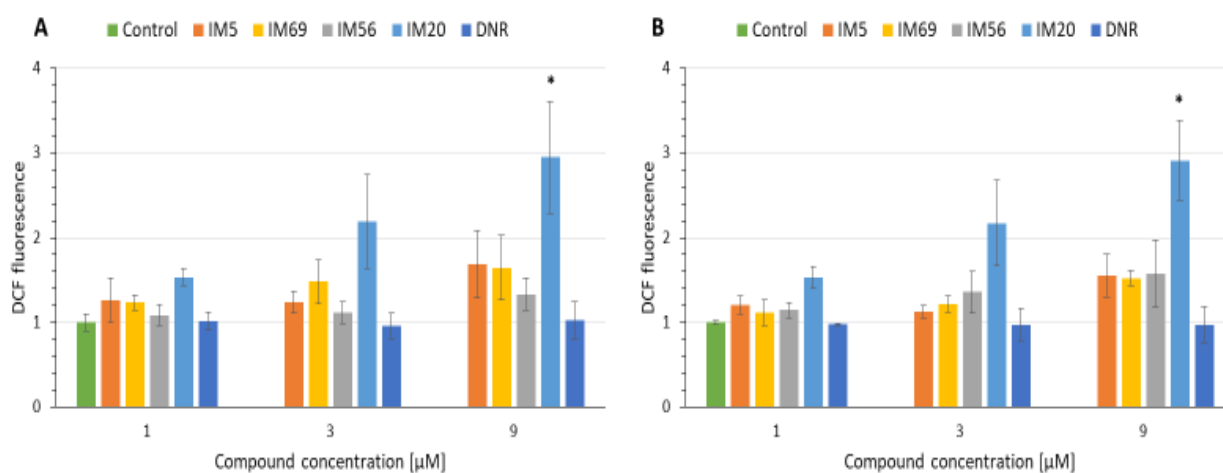


Figure 19. Iodinine-analogues induce a dose-dependent increase in DCF-signal in MOLM-13 cells. MOLM-13 cells were incubated with the indicated doses of IM 5, IM 20, IM 56 or IM 69. The doses of daunorubicin (DNR) were 0.05, 0.15 and 0.45  $\mu\text{M}$ , respectively. The generation of ROS (by DCF-fluorescence) was measured after 60 (A) and 120 (B) minutes. The green column is untreated control cells. Two experiments were performed in duplicates;  $n=4$  with standard deviation indicated by whiskers. Asterisks denote significance at  $p < 0.05$  (\*).

The generation of DCF-fluorescence was less pronounced in H9c2 compared to MOLM-13 cells (Figure 20 vs. Figure 19). IM 20 induced an increase, which was proven to be statistically significant for the concentration of 9  $\mu\text{M}$ . IM 56 induced a DCF-signal comparable to the generation in the untreated cells. IM 5 and IM 69 induced DCF-fluorescence to a lesser degree compared to untreated cells, and there was a significant decrease in DCF-signal for the treatment with 1 and 3  $\mu\text{M}$  of IM 5 and IM 69. Note the difference in y-axis in MOLM-13 cells (Figure 19) vs H9c2 cells (Figure 20) (0-4 vs 0-2). Contrary to other reports, treatment with DNR did not generate a higher DCF-signal than in untreated cells.

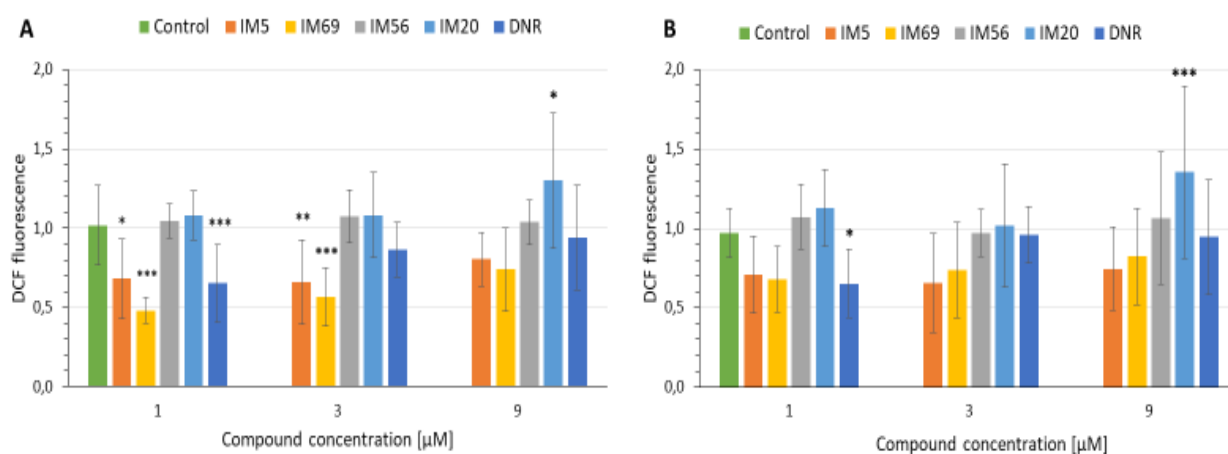


Figure 4. ROS-generation in H9c2 cells after treatment with phenazine analogues or DNR. H9c2 cells were treated with indicated doses of analogue IM 5, IM 69, IM 56, IM 20 or daunorubicin (DNR). The doses of daunorubicin (DNR) were 0.05, 0.15 and 0.45  $\mu\text{M}$ , respectively. The generation of ROS (by DCF-fluorescence) was measured after 120 (A) and 180 (B) minutes. The green column is untreated control cells. Five experiments were performed in duplicates;  $n=10$ , with standard deviation indicated by whiskers. Asterisks denote significance at  $p < 0.05$  (\*),  $<0.01$  (\*\*),  $<0.005$  (\*\*\*)

#### 4.2.2. Generation of DCF-fluorescence in MOLM-13 cells is reduced by the antioxidant N-acetyl-cysteine (NAC)

Since the cell can utilise antioxidants to protect itself against ROS-induced damage, the antioxidant N-acetyl-cysteine (NAC) was used in combination with the analogues on MOLM-13 cells to see if it induced a reduction in ROS-levels. The result from the experiment showed that the DCF fluorescence signal was reduced in the cells treated with a combination of analogue and 10 mM NAC compared to the signal from the cells treated only with analogues (Figure 21).

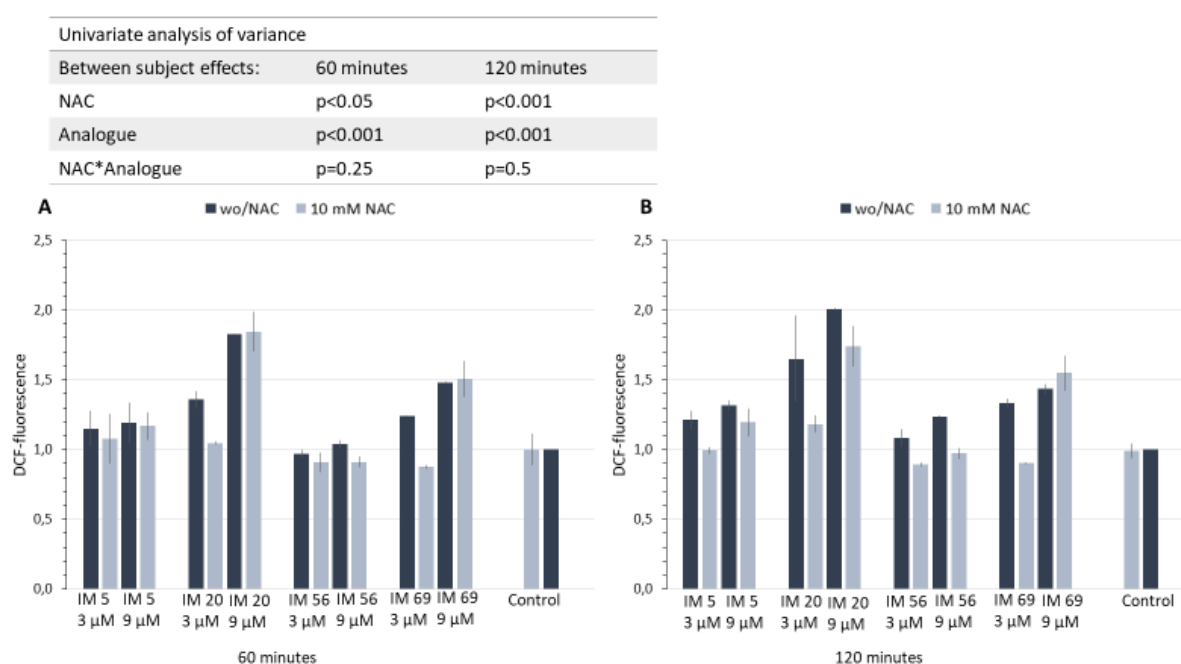


Figure 5. Co-treatment with NAC causes a significant decrease in analogue-induced ROS-production in MOLM-13 cells. The cells were treated with 3 or 9  $\mu\text{M}$  of analogue IM 5, IM 20, IM 56, and IM 69 and either co-treated with 10 mM NAC or not. The generation of ROS (by DCF fluorescence) was measured after 60 (A) and 120 (B) minutes. One experiment was performed in duplicates;  $n=2$  with top and bottom values indicated by whiskers. Table show univariate analysis of variance.

To further investigate if the cells are affected by alterations in their protection against ROS-damage, MOLM-13 cells were pre-treated with sulfasalazine (SAS) for a WST-assay, as described in section 3.6. The results of the WST-1 assay performed showed that the viability decreased (lower WST-1 signal) in MOLM-13 cells pre-treated with SAS compared to the cells only treated with analogues (Figure 22). Co-treatment with IM 56 and SAS halves the EC<sub>50</sub>-value based on WST-1 signal to ~2  $\mu$ M, relative to treatment with IM 56 only (Figure 22 A). Co-treatment with IM 20 and SAS reduces the EC<sub>50</sub>-value from ~1.7  $\mu$ M to 1.2  $\mu$ M (Figure 22 B). For IM 5 the treatments did not reach the EC<sub>50</sub>-value (Figure 22 C).

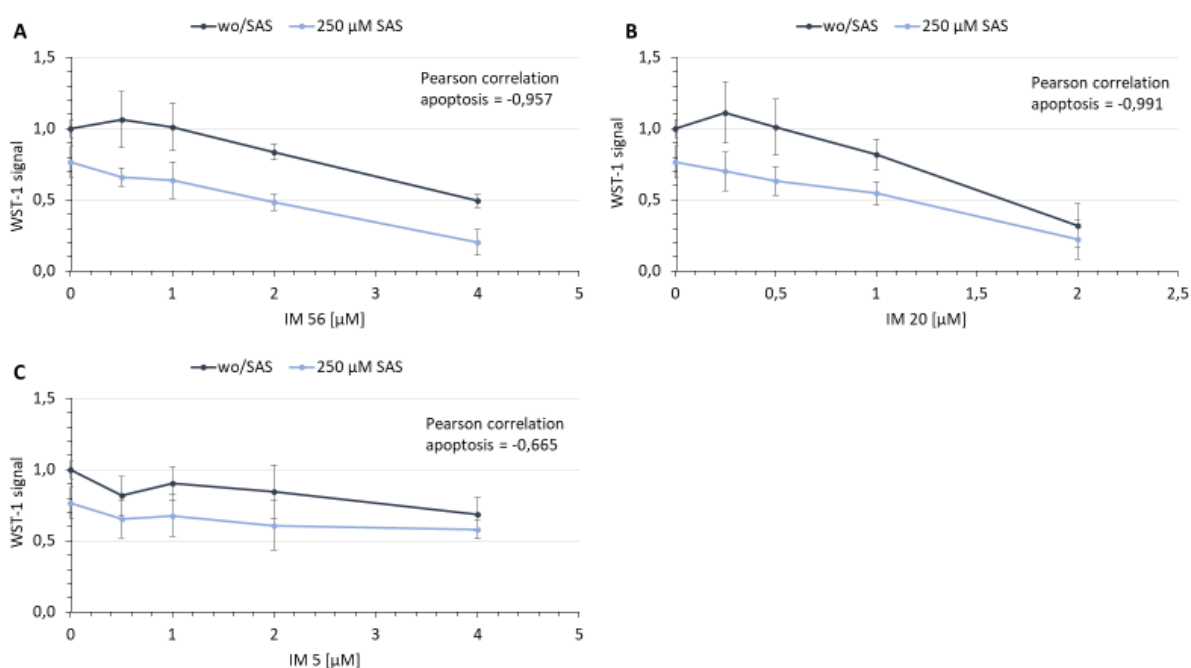
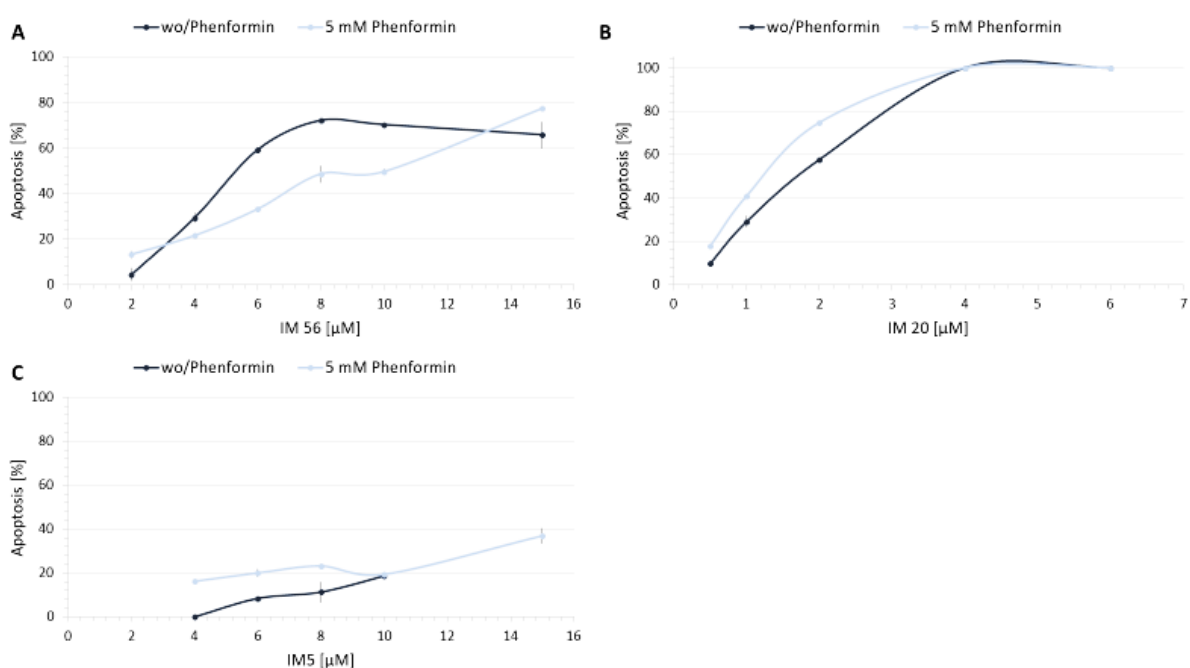


Figure 22. Pre-treatment with sulfasalazine (SAS) prior to treatment with analogues causes a decrease in metabolic activity MOLM-13 cells, relative to cells treated with an analogue only. Cells were seeded in 96-well plates as 10 000 cells/well. Half of the cells were pre-treated with 250  $\mu$ M sulfasalazine (SAS) for 24 hours. SAS was removed, and the cells were incubated the indicated doses of IM 56 (A), IM 20 (B) or IM 5 (C) for 24 hours and analysed by WST-1 assay. Two experiments were performed in duplicates;  $n=4$  with stdev. indicated by whiskers. Results from WST-1 assay was confirmed by counting living and apoptotic/dead cells by fixing cells in a 2% buffered formaldehyde solution added Hoechst 33342 stain as described in section 3.6.

We suspected that the analogues might affect the respiratory chain in the mitochondria of the cells by ROS-induction as a part of its mechanism of action. To investigate this, MOLM-13 cells were co-treated with the analogues and an inhibitor of complex I, Phenformin (31, 72) to investigate if any additional effect could be observed (Figure 23). Co-treatment with IM 56 and 5 mM phenformin increased the viability (reduced apoptosis) for IM 56-doses between 4 and 13  $\mu\text{M}$  relative to treatment with IM 56 only (Figure 23 A). The viability was decreased for co-treatment with 5 mM phenformin and analogue IM 20 (Figure 23 B) and IM 5 (Figure 23 C) relative to treatment of IM 20 and IM 5 only.



*Figure 23.6 Phenformin affects the viability of analogue-induced apoptosis in MOLM-13 cells. MOLM-13 cells were treated with the indicated concentrations of analogue IM 56 (A), IM 20 (B) and IM 5 (C), and half of them were in addition treated with 5 mM phenformin for 4 hours before a 2% buffered formaldehyde solution added Hoechst 33342 staining was added to each well. Percent apoptosis was determined by manual counting of cells and is shown relative to apoptosis in untreated cells. One experiment was performed in duplicates;  $n=2$  with top and bottom values indicated by whiskers.*

#### 4.3. Investigation of the cell signalling pathways susceptible to ROS-generation

As the induction of ROS-generation appeared to be a part of the mechanism of action for the iodinin analogues (Figure 21 and 23), we wanted to see if there was a change in the proteins known to be susceptible to alterations of ROS-levels in the cell.

As shown in Figure 24, the amount of phosphorylated AMPK $\alpha$  relative to total AMPK $\alpha$  is decreased in MOLM-13 cells treated with IM 5 and IM 56, with the most pronounced reduction in the cells treated with IM 56 for 3 hours. The amount of pAMPK $\alpha$  was increased in the cells treated with phenformin, in agreement with other studies (70). We also noted that the total amount of AMPK $\alpha$  decreased in cells treated with high concentrations of IM 56, but to a lesser degree in cells treated with high concentrations of IM 5 (Figure 24).

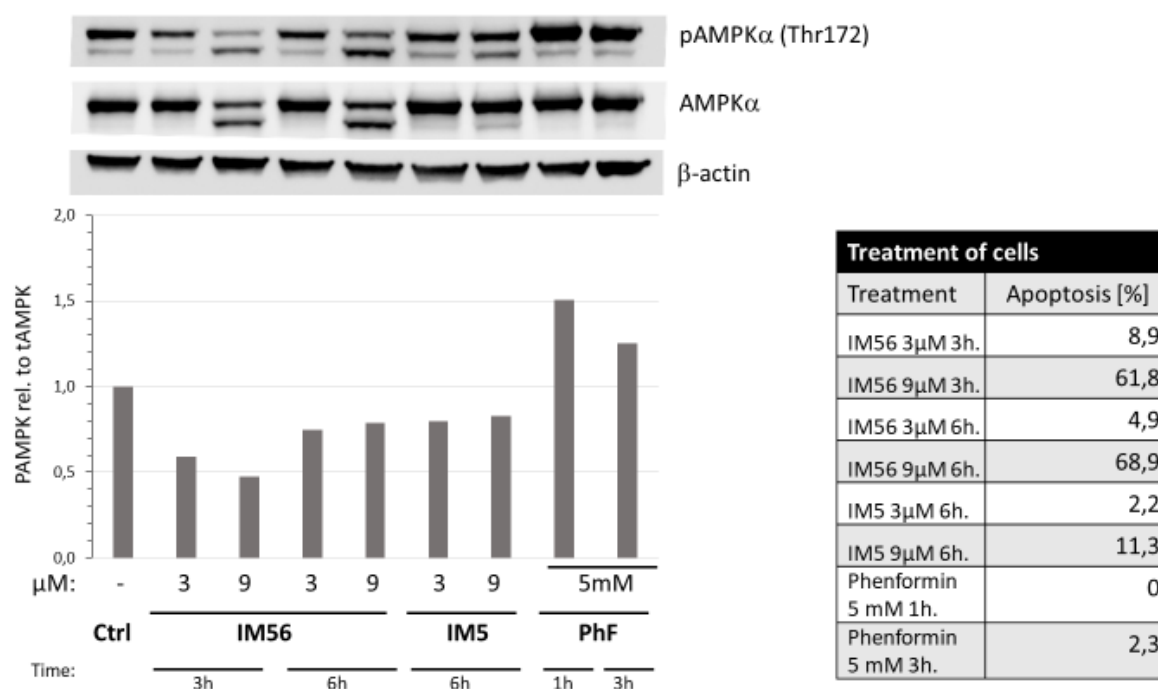
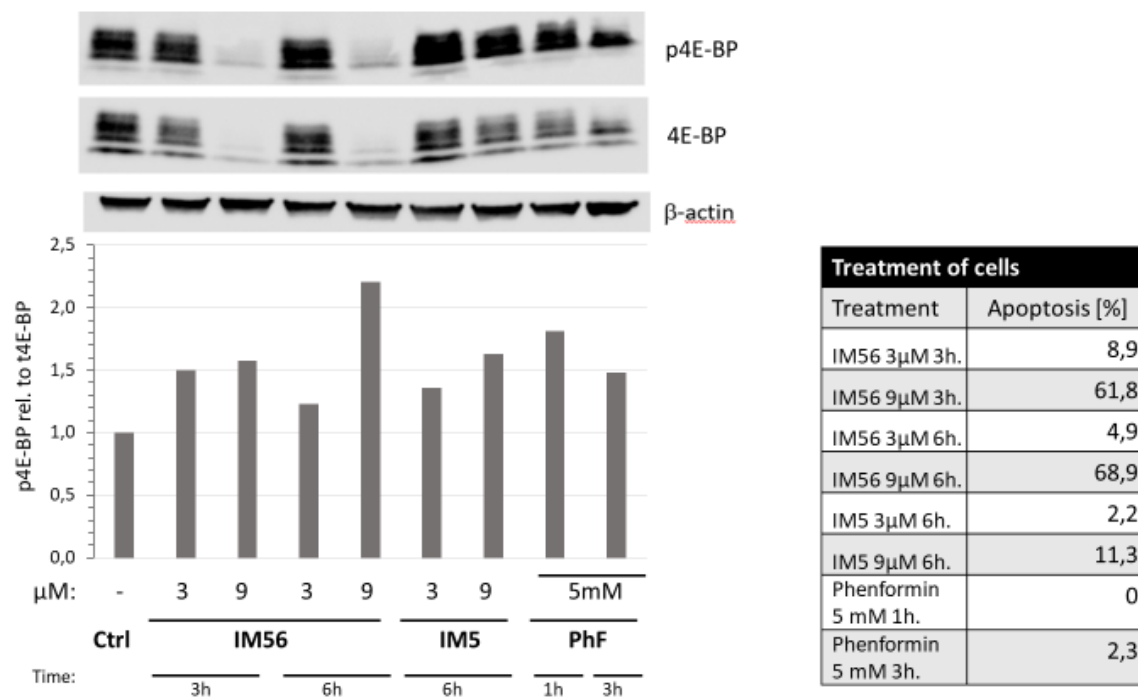


Figure 24. Iodinin and its analogue IM 56 cause a decrease in phosphorylation of AMPK $\alpha$ . MOLM-13 cells were incubated with IM 56 for 3 and 6 hours, at a concentration of 3 and 9  $\mu$ M, or with IM 5 for 6 hours at the same concentrations. Two cell conditions were treated with 5 mM phenformin for 1 and 3 hours. Samples from each condition were transferred to fix-solution and percent apoptosis was assessed as described in section 3.6. Western blotting was performed as described in section 3.8, and the membrane was incubated with antibodies for pAMPK $\alpha$  and AMPK $\alpha$ , with  $\beta$ -actin as loading control (see Table 3). The graph shows amount of phosphorylated AMPK $\alpha$  relative to total AMPK $\alpha$  in treated cells relative to an untreated control. The table show percent apoptosis relative to untreated control.



The translation initiation factor 4E-binding protein (4E-BP) is placed downstream from AMPK and mTOR and is important to regulate protein synthesis (16). The amount of phosphorylated 4E-BP increases relative to the total 4E-BP in all samples (Figure 25). Although there was an increase in the phosphorylated form of 4E-BP relative to the total protein when MOLM13 cells were treated with 9  $\mu$ M IM 56 for either 3 or 6 hours, the protein was almost totally absent compared to  $\beta$ -actin (Figure 25).



Treatment of cells	
Treatment	Apoptosis [%]
IM56 3 $\mu$ M 3h.	8,9
IM56 9 $\mu$ M 3h.	61,8
IM56 3 $\mu$ M 6h.	4,9
IM56 9 $\mu$ M 6h.	68,9
IM5 3 $\mu$ M 6h.	2,2
IM5 9 $\mu$ M 6h.	11,3
Phenformin 5 mM 1h.	0
Phenformin 5 mM 3h.	2,3

Figure 75. Iodinine and its analogue IM 56 affect 4E-BP expression in MOLM-13 cells. Results from incubating the same membrane as in Figure 24. The membrane was incubated with antibodies for phosphorylated 4E-BP and total 4E-BP, with  $\beta$ -actin as loading control (see Table 3). The graph shows amount of phosphorylated 4E-BP relative to amount of total 4E-BP in treated cells relative to an untreated control. The table shows percent apoptosis relative to untreated control.

## 5. Discussion

In this study we have provided experimental documentation on possible lead candidates for AML therapy, based on analogues derived from the previously discovered hit compound phenazine 5,10-dioxide (iodinin). Several analogues had already been tested for effect in one AML cell line and two normal cell lines, and the findings of physiochemical properties and biological activity presented herein has led to the selection of analogue IM 56 as the most promising lead. This conclusion is based on the analogue's increased cytotoxicity to AML cell lines relative to normal cell lines, and suitable results from the permeability assay.

The first property to be investigated was the analogue's ability to cross biological membranes. The permeability assay can explain why some of the analogues show more desirable effects in cell assays than others and can also predict how the analogues will interact with cell membranes or other lipid structures in the body. The analogues focused on in this project represented three of the four categories of permeability (Figure 7). The parent compound, IM 5, was classified as an intermediate permeability compound, the analogues IM 20 and IM 69 as high permeability compounds, and IM 56 as a low permeability compound.

Of all of the analogues, IM 20 was the most potent against the AML cell lines (Table 3) and the PAMPA assay showed that IM 20 had high ability to passively diffuse across a phospholipid membrane (Figure 7). It will therefore rapidly reach the critical intracellular concentration needed to disturb the cell signalling and initiate the apoptotic process. This implicates that the ability an analogue has to cross cell membranes can affect its ability to induce a cytotoxic effect in cells.

The rapid diffusion across cell membranes can also be a negative feature, as the analogue will diffuse rapidly into normal cells as well. As shown in Table 3, analogues IM 20 and IM 69, which both were classified as high permeable analogues, also have the highest potency against the cell lines representing normal tissue, namely the NRK epithelial cells and H9c2 cardiomyoblasts. Since cardiotoxicity is a common and severe side effect of the standard AML treatment utilising anthracyclines (*e.g.* Daunorubicin), a desirable effect of any new compound against AML would be to not affect heart function negatively.

One issue with IM 20 which can hamper its further development as a drug candidate, is the substituents. As shown in Figure 4 IM 20 has an ester moiety as its R<sub>2</sub> substituent. Esters are rapidly hydrolysed, and if this substituent is cleaved off, the resulting molecule is identical to

analogue IM 18 (structure shown in Supporting Table 2). As shown in Figure 7, the PAMPA assay classifies IM 18 as an impermeable compound, and Viktorsson et al. has shown that the EC<sub>50</sub> value of IM 18 in MOLM-13 cells is >50 µM in both normoxia and hypoxia (35) (Supporting Table 2). It is likely that IM 20 will be converted into IM 18 before it reaches AML cells, especially if administered orally, as it would have to withstand hydrolysis both in the gastrointestinal tract, and the first pass metabolism in the epithelial cells in the intestine and in the liver.

Another issue with IM 20 is, as mentioned above, that it is more potent against H9c2 cells than *e.g.* IM 56 (Table 5). This could possibly be explained by its rapid diffusion, but it could also be a result of a degradation of IM 20, if the degradation products are cytotoxic or the reaction itself induces cytotoxicity, for instance by generation of ROS.

Even though IM 56 has a higher cytotoxic effect on AML cell lines than IM 5 itself, it was found to have a low permeability in the PAMPA assay, while IM 5 had an intermediate permeability (Figure 7).

The low permeability of IM 56 might explain why it is less potent than IM 20 and IM 69 in the viability assay performed on OCI-AML-3 cells (Table 5). As IM 56 also showed less toxicity towards the normal cell lines, it is possible to hypothesise that the potency of the high permeability compounds makes the therapeutic window of IM 20 and IM 69 too narrow to safely use them as drugs. The parent compound, IM 5, showed an effective permeability similar to IM 56 (Figure 7), but showed less toxicity against the AML cell lines than IM 56 (Table 5).

The analogue IM 23 was used as a negative control in the liposome assay, as it had shown poor activity in previous cell assays (EC<sub>50</sub> = 50 ± 0.4 µM in MOLM-13 in normoxic conditions). HPLC-analysis of pure IM 23 diluted in acetonitrile and milliQ H<sub>2</sub>O for the standard curve used for the liposome assay gave a chromatogram which resembled the chromatogram for IM 20, shown in Figure 8. However, the analysis of the samples from the donor and acceptor well of IM 23 in the PAMPA assay gave a different result, as shown in Figure 9. The sample from the donor well eluted as several peaks, and it was not possible to separate the peaks. The chromatogram of the acceptor well showed that only small amounts of the analogue had been able to diffuse through the phospholipid membrane, and calculations from the assay classified IM 23 as impermeable (Figure 7). The structures of IM 20 and IM 23 (Figure 4 and 26 respectively), differ only by that the carbon before the carbonyl-group in

the R<sub>2</sub> substituent has been removed in the structure of IM 23, but this difference clearly has a significant impact on the physicochemical properties of the analogue.

A possible explanation to the different behaviour in the PAMPA and cytotoxicity assay is that IM 23 forms complexes when diluted in phosphate buffered saline (PBS). PBS contains Na<sup>+</sup> and K<sup>+</sup> that can form a complex with IM 23, as proposed in Figure 26. This is similar to the complex formation known to happen between the tetracycline class of antibiotics and metal ions (88). A possible reason to why this happens in IM 23 and not in IM 20 is that the carbon atom missing in IM 23 shields the electrons in the ring-structure from being pulled by the carbonyl unit and therefore avoids destabilisation of the rings.

The possible complex(es) formed are either too large or charged to be able to cross the phospholipid membrane in the PAMPA assay, as shown by the minute amounts of IM 23 present in the acceptor well of IM 23 (Figure 9). If IM 23 forms complexes in a simple buffer like PBS, it is likely to do so also in cell culture medium, which can explain why it is not active towards either cell line investigated. Moreover, body fluids like the blood contains high amounts of cationic metal ions and complexation of IM 23 is likely to occur. The PAMPA and HPLC-analyses thus explains why IM 23 is not active against AML cells, although it is very similar to the active compound IM 20.

Although the analogues' ability to cross membranes is predicted in the PAMPA assay, it does not allow us to determine if an analogue is associated with the membrane without crossing it. The liposome assay (section 4.1.2-3) was performed to investigate to what extent the analogues could be internalised in liposomes and their membrane. The results from the liposome assay can be interpreted as a permeability assay, but liposomes are also an administration formulation for anti-cancer drugs (89). IM 5 showed high liposome association (17.2%) but low loading efficiency, and it is not clear if the analogue is internalised into the liposomes or adsorbed onto the surface. This needs to be clarified before a possible liposomal

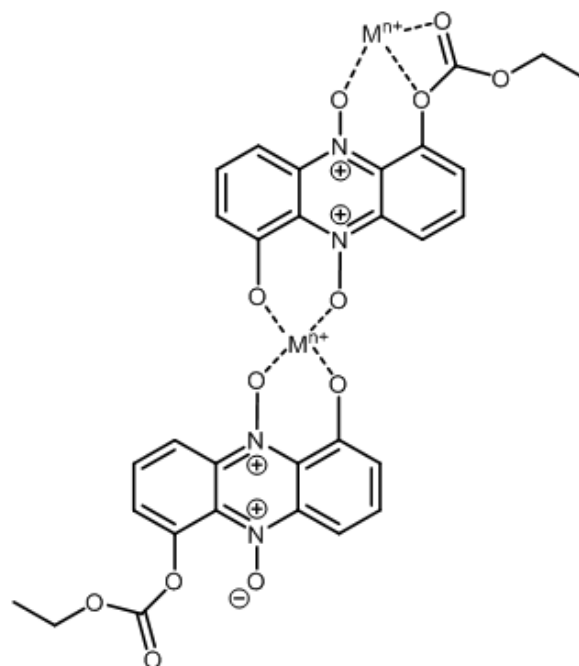


Figure 26. Proposed mechanism for complex-formation of two molecules of IM 23 with a cationic compound (M).

formulation of IM 5 can be tested for biological activity. If it is eligible, a future drug formulation would be to administer the analogue encapsulated in liposomes, which ideally has a high affinity to target AML cells.

The permeability assay gives information about how much of the compound crossed over to the acceptor plate, relative to the donor plate, whereas in the liposome assay it is not possible to differ between how much compound that have crossed completely over the membrane, and how much of the compound that is associated with the membrane.

This show a significant difference between the two assays; the artificial membrane assay will only give information about the drugs that cross the membrane into the acceptor plate, whereas the liposome assay also includes the compounds that interacts with the membrane without crossing, such as insertion between the phospholipids. This can be of importance when studying new compounds, where the mechanism of action is unknown. If the compound does not cross the membrane, but interacts with cell membranes, like IM 23, it can associate with the cell membrane of blood cells, blood plates and lipoproteins. This can give information on how a drug is transported in the blood, and further its biodistribution in the body. For example, the ester group of IM 20 is likely to degrade into the carboxylic acid moiety of IM 18 (Supporting Table 2), and will thus be charged in the blood, and susceptible for renal excretion. More lipophilic drugs, like IM 56 and IM 69, will bind to lipoproteins and be distributed into adipose and hepatic tissue. This can lengthen the drugs half-life in the body compared to hydrophilic drugs, and it will be more susceptible to hepatic clearance (37).

It is important to consider that both assays only show passive diffusion over the membrane, and that the drug can be internalized in a cell trough active transport as well. In the PAMPA assay, Daunorubicin was classified as an impermeable compound, but its high activity in cell assays suggest an active transport over the cell membrane, which also has been proven in previous literature (44). It is also possible that the analogues could be subjects of active transport, which will alter their rate of internalisation in a cell. The permeability of IM 56 was classified as low, but the cytotoxicity is comparable to that of IM 20 (Table 5). This could mean that IM 56 is in fact more potent than IM 20, but is unable to reach the inside of the cell to the same extent as IM 20. This theory is possible to test by performing an assay microinjecting IM 56 into the cell.

There was found no correlation between the effective permeability and clogP (Figure 12) or tPSA (Figure 13) for all analogues, or between  $\log P_{\text{eff}}$  and clogP for the analogues containing

the piperazine unit like IM 56 (Figure 14). There was a correlation between  $\log P_{\text{eff}}$  and tPSA for the piperazine-containing analogues (Figure 15). One can question the reliability of these findings, since the *in silico* prediction of chemical properties of structures like phenazines, where the distribution of charge between the atoms is not fixed, tends to be difficult to handle for computer software. Drugs belonging to the phenothiazine class, which has a similar three-ring system as phenazines, where one of the N-atoms is changed to a S-atom, has been referred to as “heavy outliers” in literature comparing experimental and calculated log P (90). A possible improvement of the prediction could have been gained by using the distribution coefficient, log D, instead of the partition coefficient, clog P. Log D is the overall ratio of the drug partitioned between the organic and aqueous phase, describing a drug’s lipophilicity at a fixed pH (91). The distribution of charge in a molecule changes by changing pH, and thus choosing a fixed pH (*e.g.* 7.4) could make it easier to predict the chemical properties.

In this thesis, two different methods were used for assessment of cell viability. Comparing WST-1 results with results from manual counting of apoptotic cells (Figure 17 and 18), show good correlation, which support the use of WST-1 as a satisfactory method to assess viability for these analogues. In most cases, the  $EC_{50}$ -value was higher when measuring metabolic activity compared to counting apoptotic cells (Figures 17 1-5A vs. 17 1-5B for normoxia and Figures 18 1-5A vs. 18 1-5B for hypoxia). This can be explained by that some of the pre-apoptotic cells still have intact mitochondria and metabolic activity which is registered by the WST-1 assay, but when studied in a microscope their nuclei appear apoptotic. Moreover, apoptotic and other cell deaths are associated with increased ROS levels in the cytoplasm, which can contribute to the conversion of WST-1 to the formazan product (92).

An important property of a drug is its therapeutic window. Ideally, this should be as large as possible to ensure good therapeutic effect without unacceptable side-effects. For anthracyclines, it is relevant to compare its effect on AML-cells with that on cells from the heart.

The viability studies performed on OCI-AML-3 cells, as well as previous findings (35), showed that daunorubicin (DNR) is more potent than the phenazine analogues (Table 5). However, daunorubicin has a high toxicity towards cardiomyoblasts compared to the analogues. For IM 5 and 56, there is a larger difference in  $EC_{50}$  between AML cells and cardiomyoblasts compared to daunorubicin (Table 5). This points towards that IM 5 or IM 56 can be used for AML with less chance for cardiac failure.

As shown in Table 5, the analogues are in general more potent in hypoxic conditions than in normoxic conditions. Tumours tend to be less perfused than normal tissue, and therefore have a hypoxic environment. AML is a cancer that does not form solid tumours, but there is evidence that the bone marrow has niches where there is a hypoxic environment, and that the AML cells residing here give rise to relapses (93, 94). Drugs with increased activity in hypoxic conditions will thus act stronger in the hypoxic niches where resistant AML cells reside, but less on the normal tissues, which also are sensitive to cytostatics, like the heart, peripheral blood, and intestine.

For the highest doses of analogues, especially with IM 20, it was sometimes challenging to differentiate between normal and apoptotic nuclei in the microscope. One explanation can be that cells die very rapidly, such that the classic signs of apoptosis do not have time to develop. This has previously been demonstrated in AML cell lines treated with anthracyclines and a protein synthesis inhibitor (62).

Since as a possible mechanism of action for phenazine class compounds involves the mitochondrial respiratory chain (35), the detection of generation of reactive oxygen species (ROS) is central in order to understand the mechanism, and also to be able to select a lead candidate.

The DCF-DA ROS detecting assay performed on MOLM-13 cells (Figure 19) showed an increase in DCF-signal relative to the control induced by all analogues tested, although only the highest concentration of IM 20 was proven give significant higher DCF-signal. The increase was largest for IM 20 compared to the other analogues, which also supports the previous findings that the analogue permeates the cell rapidly and is highly potent. The increase in DCF-signal appears to be dose dependent, and does not increase over time, as the DCF-signal is similar for both 60 (Figure 19 A) and 120 minutes (Figure 19 B). IM 69 induced a lower increase in DCF-signal than IM 20, but also showed no increase over time. Since IM 20 and IM 69 rapidly diffuse across membranes (Figure 7), it is likely that they reach the necessary concentration to generate maximum ROS production before the first recording after 60 minutes.

On the other hand, the generation of DCF-signal induced by IM 56 increased with higher concentrations of IM 56, and the signal is higher after 120 minutes (Figure 19 A) than after 60 minutes (Figure 19 B). The delay in ROS generation compared to IM 20 can be explained by

that IM 56 has lower permeability (Figure 7), and thus needs more time in order to reach a critical intracellular concentration.

The generation of DCF-signal induced by IM 5 appears to be quite similar to IM 69, with higher DCF-signal at 60 minutes (Figure 19 A) relatively to 120 minutes (Figure 19 B). The permeability assay classifies IM 5 as intermediate to low permeability (Figure 7), which can explain why its effect is in between that of IM 56 and IM 69. The EC<sub>50</sub>-values presented in Table 5 show that IM 5 is less potent than the other analogues. This might explain why there appears to be a leap in the DCF-signal induced by IM 5 from 1 and 3  $\mu$ M to 9  $\mu$ M (Figure 19).

The H9c2 cells (Figure 20) show a less pronounced generation of ROS relative to MOLM-13 cells (Figure 19). IM 20 induces the highest DCF-signal, most pronounced at a concentration of 9  $\mu$ M, which is supported by the EC<sub>50</sub>- values showing IM 20 is more potent in H9c2 cells relative to IM 5 and IM 56 (Table 5). The DCF-signal induced by IM 5 is low, which also is reflected by the EC<sub>50</sub> -value (>50 in H9c2 cells). Surprisingly, DNR did not induce an increase in the DCF-signal relative to the control cells. A possible explanation could be that DNR needs to be transported into the cell, and that it reaches maximum level on a later time-point than the last reading at 180 minutes. IM 69 was also expected to increase ROS based on the viability assays, but it showed a decrease in DCF-signal, which was proven to be statistically significant for 1  $\mu$ M and 3  $\mu$ M after 120 minutes (Figure 20A). The signal increased after 180 minutes (Figure 20 B), which suggests that the induction of ROS in H9c2 cells by IM 69 is slower than IM 20, even if they are both highly permeable.

To further investigate the effect of ROS-generation in the cells we tried to manipulate the cells mechanisms against ROS-induced damage in two different ways. First, by treating the cells with an anti-oxidant to see if this could lower the ROS production, and secondly by pre-treating the cells with a drug that depletes them of one of their natural antioxidants.

The treatment of MOLM-13 cells with a combination of the antioxidant N-acetyl-cysteine (NAC) led to a statistically significant overall decrease in DCF-signal relative to the DCF-signal from cells treated only with analogues (Figure 21).

Pre-treating MOLM-13 cells with sulfasalazine (SAS) was hypothesised to reduce the viability of cells, since it is known to deplete the cell of cysteine, a pre-cursor to the antioxidant glutathione, and thus sensitise the cells to ROS-mediated death (95). The reduction in viability seen with for instance IM 56 (Figure 22 A) supports that glutathione



could act as a protector to apoptosis induced by phenazine analogues. However, the concentrations of analogues used in this experiment were not sufficient for reducing the viability to zero, and further work should also observe the ROS-production by DCF-DA assay in cells co-treated with SAS and the phenazine analogues. Still, we can conclude that ROS generation is pivotal in AML cell death generated by phenazine-analogues, as demonstrated by the reduced DCF-signal in cells treated with NAC, and increased cell death in cells with blocked uptake of glutathione precursor.

Treating the cells with IM 5 and IM 56 induced a reduction in the levels of phosphorylated AMP-activated protein kinase (AMPK) compared to the total level of AMPK (Figure 24). This is expected to lead to an increase in mTOR activation, followed by an increase in mTOR-mediated phosphorylation of 4E-BP. We detected an increase in phosphorylated 4E-BP relative to the total protein for all treatments used (Figure 25). Treatment with 9  $\mu$ M IM 56 for 3 or 6 hours led to an almost complete degradation of the protein. This might be caused by the high percentage of apoptotic cells in these samples (61.8% and 68.9%).

The drug phenformin (PhF) is known to inhibit complex I of the respiratory chain in the mitochondria and this is also a location where the cell generates ROS (31, 72). In the western blot it was used as a positive control for phosphorylation of AMPK. As the treatment with IM 5 and IM 56 led to a reduction of AMPK, a combination treatment was tested (Figure 23) to investigate if the opposite effects would affect the viability. The combination treatment resulted in more apoptosis for analogue IM 5 (Figure 23 C) and IM 20 (Figure 23 B), but surprisingly not for IM 56 (Figure 23 A), where the combination treatment decreased the apoptosis. This might suggest that IM 56 have a different mechanism of action compared to IM 5 and IM 20, which also can be indicated by the results from western blotting for 4E-BP (Figure 25). Here, the highest concentration of IM 56 (9  $\mu$ M), almost completely knocked down the expression of 4E-BP. The total AMPK-expression is also altered for this concentration, (Figure 24), which might support this theory. This additional effect could be caused by the piperazine R<sub>1</sub>-substituent (Figure 4), which is absent on both IM 5 and IM 20. If this is the case, similar results should be obtained with IM 69, since it has the same piperazine substituent as IM 56 (Figure 4).

Interestingly, treatment of cells with phenformin affected phosphorylation of 4E-BP oppositely compared to what was seen with the analogues; the strong activation of AMPK by phenformin (Figure 24), would be expected to decrease the phosphorylation of 4E-BP, but as shown in Figure 25, this treatment lead to an increase.

Protein kinase B (AKT) (Supporting Figure 2) protein S6 kinase (P70S6K) (Supporting Figure 1) were not changed relative to the total protein, but the level of total protein was lowered with all treatments. However, the quality of these blots is not sufficient to draw final conclusions. The total protein was lowest in two of the lanes with highest percent apoptosis (lane 4 and 7), but not for lane 5, which also had a high percentage of apoptosis. Taken together, the western blots showed that both 4E-BP, AKT and P70S6K is degraded compared to  $\beta$ -actin. This points towards degradation of these proteins, but not degradation of cytoskeletal components, either by apoptosis initiated by caspase cleavage, or by lysosomal degradation by autophagy.

The first report on iodinin and AML showed cleavage of procaspase 9 into active caspase 9 (87). In order to find if autophagic mechanisms are activated, specific markers like LC3 should be investigated. The dephosphorylation of AMPK is generally associated with impaired autophagic function (96). In order to conclude further from the western blots with AKT and P70S6K, they should be repeated to ensure that protein loading is similar. Furthermore, to exclude cell death mediated protein degradation, lower concentrations of cytotoxic agents must be used.

Future studies should also investigation of mTOR, from the same cell lysate preparation in order to find if this is the mediator of down-stream effects of AMPK dephosphorylation. If this is the case, a combination treatment with an mTOR inhibitor and for instance IM 56 could give a synergistic effect.

## 6. Concluding remarks

The main aim of this master thesis was to investigate the biological activity and physiochemical properties of analogues of from the phenazine 5,10-dioxide, iodinin, to be able to choose one analogue with superior drug properties for further clinical studies. The information obtained in this work, together with previous findings, led to the selection of IM 56 as the most promising candidate for future drug development.

This conclusion is based on the favourable results shown for IM 56 over the other analogues. Most importantly, it showed enhanced cytotoxic effect towards AML cell lines compared to the parent compound, IM 5. The potency of IM 56 is lower against normal cell lines compared to the other analogues, as well as the current standard treatment, daunorubicin. It induced an increase of ROS-generation in MOLM-13 cells, but not in cardiomyoblasts.

The results of the investigation of the physiochemical properties using a permeability assay gave valuable information regarding the analogues, providing a partial explanation of the results shown in the cytotoxicity assays.

The analogue IM 20 also showed high cytotoxic effects towards AML cell lines, and could have been chosen as a drug lead, but there are some drawbacks regarding this analogue. The high cytotoxic effect is also shown towards the normal cell lines, and it induced high levels of ROS in cardiomyoblasts. It is highly permeable over phospholipid membranes, which increases the risk of undesirable side-effects. Lastly, IM 20 is likely to be susceptible to unwanted degradation to IM 18 in the body. IM 18 was shown to be inactive and impermeable.

In total, the abovementioned findings make IM 56 a better choice for a drug lead, as it is less likely to have severe side-effects compared to the more potent analogue IM 20.

The molecular mechanism of action was not found during the work for this thesis, and further studies should be performed. The results suggest that the mechanism of action includes involvement of ROS generation and modulation of the cell signalling pathways connected to AMPK. Both down-stream and up-stream factors of AMPK should be further studied to confirm this.

## 7. Further studies

Development of the analogue IM 56 into a marketable drug would require several steps, starting with further pre-clinical studies in systems that resembles the complexity of the body. Since a key point against the standard treatment with daunorubicin is cardiotoxicity, studies should be performed to reveal any possible negative effect of IM 56 in an intact heart model.

To pinpoint the molecular mechanism of action further studies should focus on investigation of how the analogue induces generation of ROS and how this affects the cell. A possible method to study the link between ROS-generation and the mitochondrial respiratory chain is utilising an assay that monitors the oxygen consumption in the mitochondria when treating the cell with the analogue. Anthracyclines induce DNA-damage by intercalation, and possible DNA-intercalation with the analogues should be investigated by direct DNA-drug interaction studies.

Since we have selected a lead compound for drug development it is natural to continue *in vivo* pharmacokinetic and pharmacodynamic studies, and thereafter efficacy studies in an animal model for AML. Preferably, the first efficacy study should be a model where MOLM-13 cells can be used, for instance by xenografts in mice.

After toxicity studies, the most suitable way to administer the analogue as a drug should be investigated. An oral route of administration would be preferred, but intravenous injections or infusions are commonly used in cancer therapy and could be chosen, depending on the dose regimen developed for the compound.

## 8. References

1. National Cancer Institute. What Is Cancer. National Cancer Institute 2018 [27.11.2017]. Available from: <https://www.cancer.gov/about-cancer/understanding/what-is-cancer>.
2. Akutt myelogen leukemi (AML): Norsk Helseinformatikk; [27.11.2017]. Available from: <https://nhi.no/sykdommer/barn/kreftsykdommer/akutt-myelogen-leukemi-oversikt/?page=all>.
3. Mehta A, Hoffbrand, V. Haematology at a Glance. 3 ed. West Sussex, UK: Wiley-Blackwell; 2009.
4. National Cancer Institute. Cancer Stat Facts: Leukemia - Acute Myeloid Leukemia (AML): National Cancer Institute; [28.11.2017]. Available from: <https://seer.cancer.gov/statfacts/html/amy1.html>.
5. De Kouchkovsky I, Abdul-Hay M. 'Acute myeloid leukemia: a comprehensive review and 2016 update'. Blood cancer journal. 2016;6(7):e441.
6. Hammerstrøm Jens et al. Nasjonalt handlingsprogram med retningslinjer for diagnostikk, behandling og oppfølging av maligne blodsykdommer. Kap. 4.11.10 Primærbehandling av pasienter over 65 år [Nasjonale retningslinjer]. Helsedirektoratet; 2012 [updated 14.10.2016; cited 07.05.2018]. Available from: <http://www.helsebiblioteket.no/retningslinjer/maligne-blodsykdommer/akutt-myelogen-leukemi-aml/behandling/prim%C3%A6rbehandling-over-65-%C3%A5r>.
7. American Cancer Society. How is Acute Myeloid Leukemia Classified? [updated 22.02.2016; cited 08.05.2018]. Available from: [https://www.cancer.org/cancer/acute-myeloid-leukemia/detection-diagnosis-staging/how-classified.html#written\\_by](https://www.cancer.org/cancer/acute-myeloid-leukemia/detection-diagnosis-staging/how-classified.html#written_by).
8. Kayser S, Schlenk RF, Londono MC, Breitenbuecher F, Wittke K, Du J, et al. Insertion of FLT3 internal tandem duplication in the tyrosine kinase domain-1 is associated with resistance to chemotherapy and inferior outcome. Blood. 2009;114(12):2386-92.
9. Hou HA, Chou WC, Kuo YY, Liu CY, Lin LI, Tseng MH, et al. TP53 mutations in de novo acute myeloid leukemia patients: longitudinal follow-ups show the mutation is stable during disease evolution. Blood cancer journal. 2015;5(7):e331.
10. Zilfou JT, Lowe SW. Tumor Suppressive Functions of p53. Cold Spring Harbor Perspectives in Biology. 2009;1(5):a001883.
11. Heath EM, Chan SM, Minden MD, Murphy T, Shlush LI, Schimmer AD. Biological and clinical consequences of NPM1 mutations in AML. Leukemia. 2017;31:798.
12. Liu Y, He P, Liu F, Shi L, Zhu H, Zhao J, et al. Prognostic significance of NPM1 mutations in acute myeloid leukemia: A meta-analysis. Molecular and Clinical Oncology. 2014;2(2):275-81.
13. Sanchez-Correa B, Bergua JM, Campos C, Gayoso I, Arcos MJ, Banas H, et al. Cytokine profiles in acute myeloid leukemia patients at diagnosis: survival is inversely correlated with IL-6 and directly correlated with IL-10 levels. Cytokine. 2013;61(3):885-91.
14. Ma XM, Blenis J. Molecular mechanisms of mTOR-mediated translational control. Nature Reviews Molecular Cell Biology. 2009;10:307.
15. Littler DR, Walker JR, Davis T, Wybenga-Groot LE, Finerty PJ, Newman E, et al. A conserved mechanism of autoinhibition for the AMPK kinase domain: ATP-binding site and catalytic loop refolding as a means of regulation. Acta Crystallographica Section F: Structural Biology and Crystallization Communications. 2010;66(Pt 2):143-51.
16. Zhang Y, Zheng XFS. mTOR-independent 4E-BP1 phosphorylation is associated with cancer resistance to mTOR kinase inhibitors. Cell Cycle. 2012;11(3):594-603.
17. Burnett PE, Barrow RK, Cohen NA, Snyder SH, Sabatini DM. RAFT1 phosphorylation of the translational regulators p70 S6 kinase and 4E-BP1. Proceedings of the National Academy of Sciences. 1998;95(4):1432-7.
18. Hammerstrøm Jens et al. Nasjonalt handlingsprogram med retningslinjer for diagnostikk, behandling og oppfølging av maligne blodsykdommer. Kap. 4 Akutt myelogen leukemi (AML), [Nasjonale Retningslinjer]. Helsedirektoratet; 2012 [updated 14.10.2016; cited 26.04.2018]. Available from: <http://www.helsebiblioteket.no/retningslinjer/maligne-blodsykdommer/akutt-myelogen-leukemi-aml>.
19. Hammerstrøm Jens et al. Nasjonalt handlingsprogram med retningslinjer for diagnostikk, behandling og oppfølging av maligne blodsykdommer. Kap. 4.9 Remisjonskriterier og prognose,

- [Nasjonale retningslinjer]. Helsedirektoratet; 2012 [updated 14.10.2016; cited 26.04.2018. Available from: <http://www.helsebiblioteket.no/retningslinjer/maligne-blodsykdommer/akutt-myelogen-leukemi-aml/remisjonskriterier-og-prognose>.
20. Peccatori J, Ciceri F. Allogeneic stem cell transplantation for acute myeloid leukemia. *Haematologica*. 2010;95(6):857-9.
  21. Singal PK, Iliskovic N. Doxorubicin-Induced Cardiomyopathy. *New England Journal of Medicine*. 1998;339(13):900-5.
  22. Van Etten R. Molecular genetics of chronic myeloid leukemia. 13.0 ed: UpToDate; 2018.
  23. National Cancer Institute. Cancer Stat Facts: Leukemia- Chronic Myeloid Leukemia (CML) 2018 [10.05.2018]. Available from: <https://seer.cancer.gov/statfacts/html/cmlyl.html>.
  24. Weisberg E, Sattler M, Manley PW, Griffin JD. Spotlight on midostaurin in the treatment of FLT3-mutated acute myeloid leukemia and systemic mastocytosis: design, development, and potential place in therapy. *OncoTargets and therapy*. 2018;11:175-82.
  25. Lancet JE, Cortes JE, Hogge DE, Tallman MS, Kovacovics TJ, Damon LE, et al. Phase 2 trial of CPX-351, a fixed 5:1 molar ratio of cytarabine/daunorubicin, vs cytarabine/daunorubicin in older adults with untreated AML. *Blood*. 2014;123(21):3239-46.
  26. Godwin CD, Gale RP, Walter RB. Gemtuzumab ozogamicin in acute myeloid leukemia. *Leukemia*. 2017;31(9):1855-68.
  27. DeStefano CB, Hourigan CS. Personalizing initial therapy in acute myeloid leukemia: incorporating novel agents into clinical practice. *Therapeutic advances in hematology*. 2018;9(5):109-21.
  28. Brown JM, Wilson WR. Exploiting tumour hypoxia in cancer treatment. *Nature Reviews Cancer*. 2004;4:437.
  29. Raza MH, Siraj S, Arshad A, Waheed U, Aldakheel F, Alduraywish S, et al. ROS-modulated therapeutic approaches in cancer treatment. *Journal of Cancer Research and Clinical Oncology*. 2017;143(9):1789-809.
  30. DeBerardinis RJ, Chandel NS. Fundamentals of cancer metabolism. *Science Advances*. 2016;2(5):e1600200.
  31. Panieri E, Santoro MM. ROS homeostasis and metabolism: a dangerous liason in cancer cells. *Cell death & disease*. 2016;7(6):e2253.
  32. Kumari S, Badana AK, G MM, G S, Malla R. Reactive Oxygen Species: A Key Constituent in Cancer Survival. *Biomarker Insights*. 2018;13:1177271918755391.
  33. U.S. Food and Drug Administration. Novel Drug Approvals for 2017 [30.11.2017]. Available from: <https://www.fda.gov/Drugs/DevelopmentApprovalProcess/DrugInnovation/ucm537040.htm>.
  34. Wikberg J, Eklund M., Willighagen E., Spjuth O., Lapins M., Engkvist O., Alvarsson J. Introduction to pharmaceutical bioinformatics. 2 ed: Oakleaf Academic Publishing House; 2010.
  35. Viktorsson EO, Melling Grothe B, Aesoy R, Sabir M, Snellingen S, Prandina A, et al. Total synthesis and antileukemic evaluations of the phenazine 5,10-dioxide natural products iodinin, myxin and their derivatives. *Bioorganic & medicinal chemistry*. 2017;25(7):2285-93.
  36. Tsopelas F, Giaginis C, Tsantili-Kakoulidou A. Lipophilicity and biomimetic properties to support drug discovery. *Expert Opinion on Drug Discovery*. 2017;12(9):885-96.
  37. Bardal S, Waechter, J., Martin, D. *Applied Pharmacology*: Elsevier; 2011.
  38. Davis J. *Chromobacterium iodinum* (n.sp.). *Zentralblatt fuer Bakteriologie, Parasitenkunde, Infektionskrankheiten und Hygiene*. 1939:273-6.
  39. McIlwain H. The anti-streptococcal action of iodinin. Naphthaquinones and anthraquinones as its main natural antagonists. *The Biochemical journal*. 1943;37(2):265-71.
  40. Hollstein U, Van Gemert RJ. Interaction of phenazines with polydeoxyribonucleotides. *Biochemistry*. 1971;10(3):497-504.
  41. Endo H, Tada M. STUDIES ON ANTITUMOR ACTIVITY OF PHENAZINE DERIVATIVES AGAINST S 180 AND C 63 IN MICE. (I). The science reports of the research institutes, Tohoku University Ser C, Medicine Tohoku Daigaku. 1965;12:53-7.
  42. Røsjø B. Molekyl fra havet dreper både blodkreftceller og resistente bakterier, 2017 29.04.2018, . Available from: <https://titan.uio.no/node/2526>.
  43. Yang NJ, Hinner MJ. Getting Across the Cell Membrane: An Overview for Small Molecules, Peptides, and Proteins. *Methods in molecular biology* (Clifton, NJ). 2015;1266:29-53.

44. Andreev E, Brosseau N, Carmona E, Mes-Masson A-M, Ramotar D. The human organic cation transporter OCT1 mediates high affinity uptake of the anticancer drug daunorubicin. *Scientific reports*. 2016;6:20508.
45. Corning Inc. Corning® Gentest™ Pre-coated PAMPA Plate System 2013 [10/13 CLS-DL-GT-023 REV1:[Available from: [https://www.corning.com/media/worldwide/cls/documents/CLS\\_DL\\_GT\\_023\\_REV1.pdf](https://www.corning.com/media/worldwide/cls/documents/CLS_DL_GT_023_REV1.pdf).
46. Bennion BJ, Be NA, McNerney MW, Lao V, Carlson EM, Valdez CA, et al. Predicting a Drug's Membrane Permeability: A Computational Model Validated With in Vitro Permeability Assay Data. *The journal of physical chemistry B*. 2017;121(20):5228-37.
47. Hitachi. Configuration of an HPLC system [26.11.2017]. Available from: <https://www.hitachi-hightech.com/global/products/science/tech/ana/lc/basic/course3.html>.
48. Hitachi. Principle of Chromatography [26.11.2017]. Available from: <https://www.hitachi-hightech.com/global/products/science/tech/ana/lc/basic/course1.html>.
49. Liposomes a practical approach. New RRC, editor. New York: Oxford University Press; 1990.
50. Akbarzadeh A, Rezaei-Sadabady R, Davaran S, Joo SW, Zarghami N, Hanifehpour Y, et al. Liposome: classification, preparation, and applications. *Nanoscale research letters*. 2013;8(1):102.
51. Sigma-Aldrich. Gel Filtration Chromatography [26.11.2017]. Available from: <https://www.sigmaaldrich.com/life-science/proteomics/protein-chromatography/gel-filtration-chromatography.html>.
52. MerckMillipore. FTIR Spectrometer Technology [26.11.2017]. Available from: <http://www.merckmillipore.com/NO/en/life-science-research/protein-detection-quantification/direct-detect-spectrometer/ftir-technology/Bi2b.qB.wJMAAFB21kRRkw8.nav#principles>.
53. MerckMillipore. Lipid Analysis with Direct Detect® Spectrometer [26.11.2017]. Available from: <https://www.merckmillipore.com/NO/en/life-science-research/protein-detection-quantification/direct-detect-spectrometer/applications/lipid-analysis/hGOB.qB.KHkAAAFB3eARRkxC.nav?ReferrerURL=https%3A%2F%2Fwww.google.no%2F&bd=1>
54. Leibniz-Institut DSMZ - Deutsche Sammlung von Mikroorganismen und Zellkulturen GmbH. MOLM-13. 2018.
55. Matsuo Y, MacLeod RAF, Uphoff CC, Drexler HG, Nishizaki C, Katayama Y, et al. Two acute monocytic leukemia (AML-M5a) cell lines (MOLM-13 and MOLM-14) with interclonal phenotypic heterogeneity showing MLL-AF9 fusion resulting from an occult chromosome insertion, ins(11;9)(q23;p22p23). *Leukemia*. 1997;11:1469.
56. Leibniz-Institut DSMZ - Deutsche Sammlung von Mikroorganismen und Zellkulturen GmbH. OCI-AML-3. 2018.
57. ATTC. H9c2(2-1) (ATCC® CRL-1446™) 2018 [17.05.2018]. Available from: [https://www.lgcstandards-atcc.org/Products/All/CRL-1446.aspx?geo\\_country=no#culturemethod](https://www.lgcstandards-atcc.org/Products/All/CRL-1446.aspx?geo_country=no#culturemethod).
58. Roche Diagnostics GmbH. Cell Proliferation Reagent WST-1. Version 16 ed: Roche; 2011.
59. Prabst K, Engelhardt H, Ringgeler S, Hubner H. Basic Colorimetric Proliferation Assays: MTT, WST, and Resazurin. *Methods in molecular biology* (Clifton, NJ). 2017;1601:1-17.
60. BioRad Laboratories Inc. PureBlu(TM) Hoechst 33342 Nuclear Staining Dye. 10043283 Rev A ed.
61. Saraste A, Pulkki K. Morphologic and biochemical hallmarks of apoptosis. *Cardiovascular research*. 2000;45(3):528-37.
62. Gausdal G, Gjertsen BT, McCormack E, Van Damme P, Hovland R, Krakstad C, et al. Abolition of stress-induced protein synthesis sensitizes leukemia cells to anthracycline-induced death. *Blood*. 2008;111(5):2866-77.
63. Felleskatalogen. Salazopyrin EN 2014 [30.04.2018,]. Available from: <https://www.felleskatalogen.no/medisin/salazopyrin-en-pfizer-563691>.
64. Lo M, Ling V, Low C, Wang YZ, Gout PW. Potential use of the anti-inflammatory drug, sulfasalazine, for targeted therapy of pancreatic cancer. *Current Oncology*. 2010;17(3):9-16.
65. Maxwell SR. Prospects for the use of antioxidant therapies. *Drugs*. 1995;49(3):345-61.
66. Felleskatalogen. Bronkyl, Bronkyl forte (Weifa): Felleskatalogen; 2017 [updated 24.02.201730.04.2018]. Available from: <https://www.felleskatalogen.no/medisin/bronkyl-bronkyl-forte-weifa-547125>.

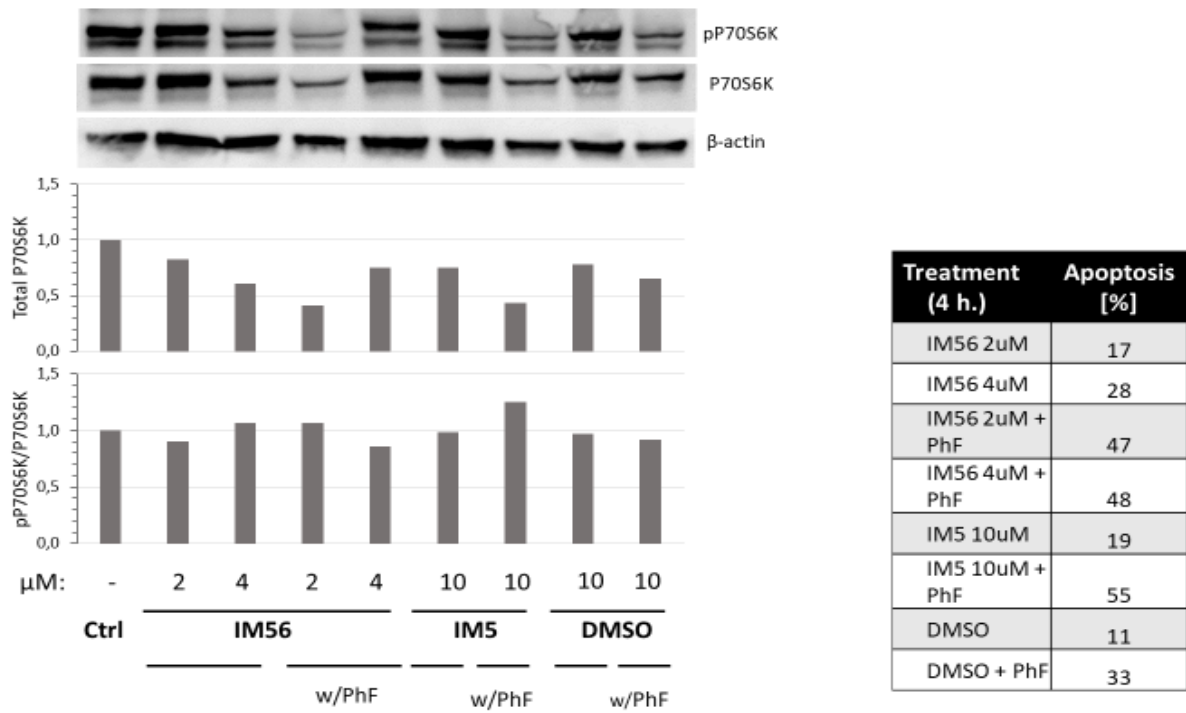
67. Sansone RA, Sansone LA. Getting a Knack for NAC: N-Acetyl-Cysteine. *Innovations in clinical neuroscience*. 2011;8(1):10-4.
68. Sagrista ML, Garcia AE, Africa De Madariaga M, Mora M. Antioxidant and pro-oxidant effect of the thiolic compounds N-acetyl-L-cysteine and glutathione against free radical-induced lipid peroxidation. *Free radical research*. 2002;36(3):329-40.
69. Miskimins WK, Ahn HJ, Kim JY, Ryu S, Jung YS, Choi JY. Synergistic anti-cancer effect of phenformin and oxamate. *PloS one*. 2014;9(1):e85576.
70. Saini N, Yang X. Metformin as an anti-cancer agent: actions and mechanisms targeting cancer stem cells. *Acta biochimica et biophysica Sinica*. 2018;50(2):133-43.
71. Ota S, Horigome K, Ishii T, Nakai M, Hayashi K, Kawamura T, et al. Metformin suppresses glucose-6-phosphatase expression by a complex I inhibition and AMPK activation-independent mechanism. *Biochemical and biophysical research communications*. 2009;388(2):311-6.
72. Wheaton WW, Weinberg SE, Hamanaka RB, Soberanes S, Sullivan LB, Anso E, et al. Metformin inhibits mitochondrial complex I of cancer cells to reduce tumorigenesis. *eLife*. 2014;3:e02242.
73. Sharma LK, Lu J, Bai Y. Mitochondrial Respiratory Complex I: Structure, Function and Implication in Human Diseases. *Current medicinal chemistry*. 2009;16(10):1266-77.
74. Sand Oea. *Menneskets fysiologi*. 2 ed. Oslo: Gyldendal Norsk Forlag AS; 2014.
75. Hardie DG. Role of AMP-activated protein kinase in the metabolic syndrome and in heart disease. *FEBS Letters*. 2008;582(1):81-9.
76. Soh N. Recent advances in fluorescent probes for the detection of reactive oxygen species. *Analytical and bioanalytical chemistry*. 2006;386(3):532-43.
77. Abcam. ab113851 DCFDA Cellular ROS Detection Assay Kit. 12 ed 2017.
78. Afzal M, Matsugo S, Sasai M, Xu B, Aoyama K, Takeuchi T. Method to overcome photoreaction, a serious drawback to the use of dichlorofluorescein in evaluation of reactive oxygen species. *Biochemical and biophysical research communications*. 2003;304(4):619-24.
79. Mahmood T, Yang PC. Western Blot: Technique, Theory, and Trouble Shooting. *North American Journal of Medical Sciences*. 2012;4(9):429-34.
80. The Human Protein Atlas. Western blot: The Human Protein Atlas; [cited 2018 14.04]. Available from: <https://www.proteinatlas.org/learn/method/western+blot#refs>.
81. Bass J. J. An overview of technical considerations for Western blotting applications to physiological research. *Scandinavian Journal of Medicine & Science in Sports*. 2017;27(1):4-25.
82. Shanler M. Automation of Pre-coated PAMPA Plates Improves Predictability, Reproducibility, and Efficiency 2012 27.11.2017. Available from: [https://catalog2.corning.com/LifeSciences/en-US/Shopping/ProductDetails.aspx?productid=353015\(Lifesciences\)](https://catalog2.corning.com/LifeSciences/en-US/Shopping/ProductDetails.aspx?productid=353015(Lifesciences)).
83. Knudsen KS. Development of nanocarriers for co-delivery of statins and anthracyclines. Bergen: University of Bergen; 2017.
84. Bradford MM. A rapid and sensitive method for the quantitation of microgram quantities of protein utilizing the principle of protein-dye binding. *Analytical Biochemistry*. 1976;72(1):248-54.
85. Bio-Rad Laboratories Inc. Quick Start™ Bradford Protein Assay Instruction Manual. Rev A ed.
86. SPSS. Pearson Correlations - Quick Introduction 2018 [11.05.2018]. Available from: <https://www.spss-tutorials.com/pearson-correlation-coefficient/>.
87. Myhren LE, Nygaard G, Gausdal G, Sletta H, Teigen K, Degnes KF, et al. Iodinine (1,6-dihydroxyphenazine 5,10-dioxide) from *Streptosporangium* sp. induces apoptosis selectively in myeloid leukemia cell lines and patient cells. *Marine drugs*. 2013;11(2):332-49.
88. Palm GJ, Lederer T, Orth P, Saenger W, Takahashi M, Hillen W, et al. Specific binding of divalent metal ions to tetracycline and to the Tet repressor/tetracycline complex. *JBIC Journal of Biological Inorganic Chemistry*. 2008;13(7):1097.
89. Bulbake U, Doppalapudi S, Kommineni N, Khan W. Liposomal Formulations in Clinical Use: An Updated Review. *Pharmaceutics*. 2017;9(2):12.
90. Eros D, Kovédi I, Orfi L, Takacs-Novak K, Acsády G, Keri G. Reliability of logP predictions based on calculated molecular descriptors: a critical review. *Curr Med Chem*. 2002;9(20):1819-29.



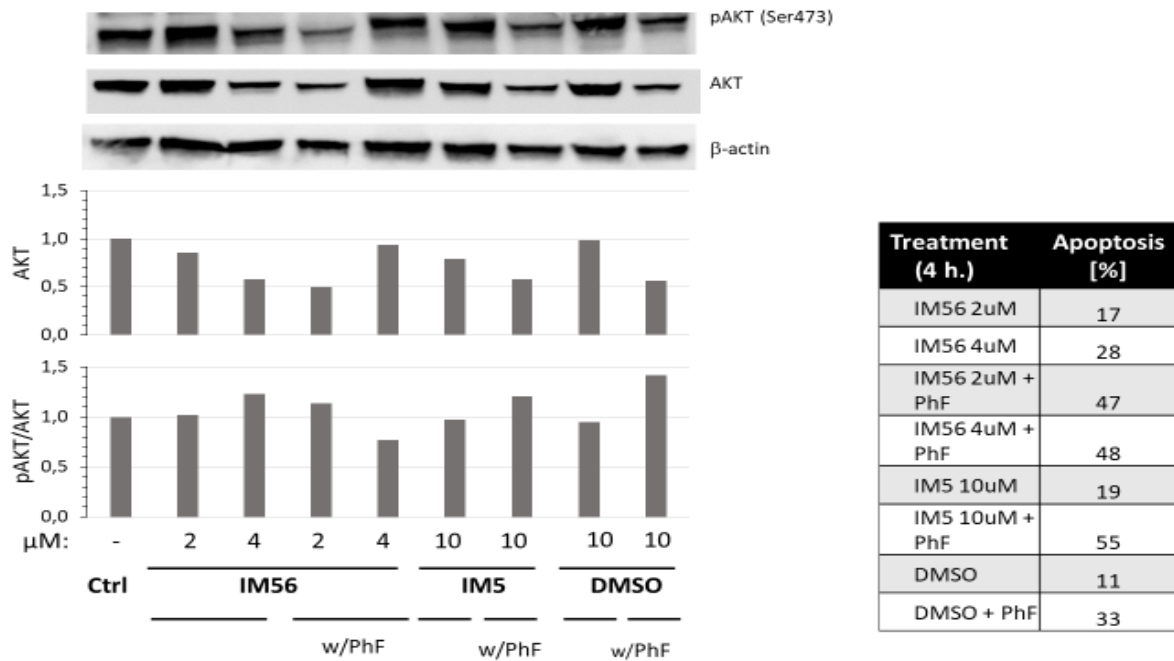
91. Manners CN, Payling DW, Smith DA. Distribution coefficient, a convenient term for the relation of predictable physico-chemical properties to metabolic processes. *Xenobiotica*. 1988;18(3):331-50.
92. Mandal S, Hazra B, Sarkar R, Biswas S, Mandal N. Assessment of the Antioxidant and Reactive Oxygen Species Scavenging Activity of Methanolic Extract of *Caesalpinia crista* Leaf. *Evidence-based Complementary and Alternative Medicine : eCAM*. 2011;2011:173768.
93. Jin L, Tabe Y, Zhou Y, Miida T, Andreeff M, Konopleva M. Efficacy and Mechanisms of Apoptosis Induction by Simultaneous Inhibition of PI3K with GDC-0941 and Blockade of Bcl-2 (ABT-737) or FLT3 (Sorafenib) In AML Cells In the Hypoxic Bone Marrow Microenvironment. *Blood*. 2010;116(21):777-.
94. Zhou HS, Carter BZ, Andreeff M. Bone marrow niche-mediated survival of leukemia stem cells in acute myeloid leukemia: Yin and Yang. *Cancer biology & medicine*. 2016;13(2):248-59.
95. Skeie B. Gamma knife surgery for intracranial tumours – clinical and experimental studies. Bergen: University of Bergen; 2014.
96. Wang Z, Liu P, Chen Q, Deng S, Liu X, Situ H, et al. Targeting AMPK Signaling Pathway to Overcome Drug Resistance for Cancer Therapy. *Current drug targets*. 2016;17(8):853-64.

# Appendix I

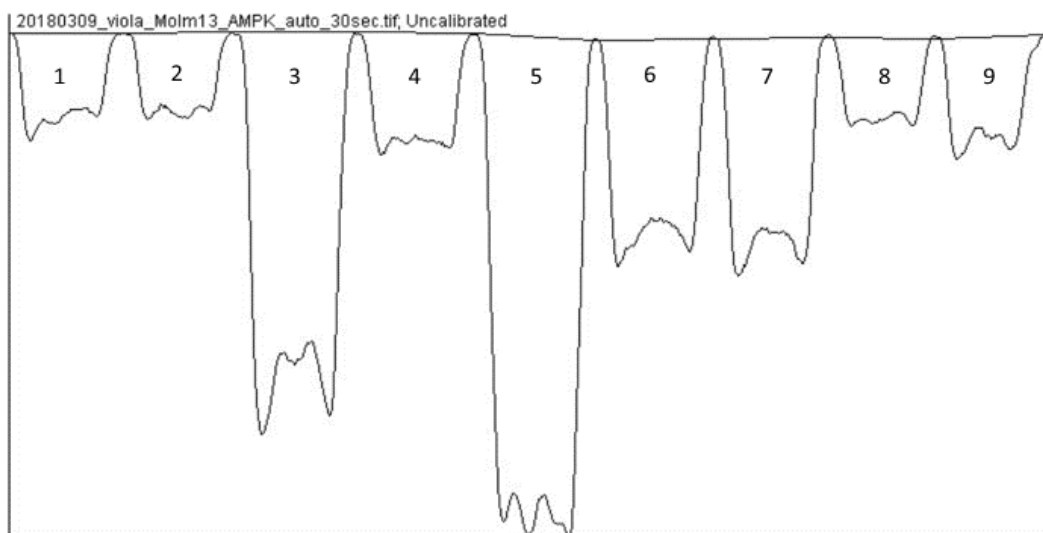
## Supporting Figures



Supporting Figure 1. Western blot for pP70S6K and P70S6K. MOLM-13 cells were incubated with IM 56, IM 5 and DMSO for 4 hours, at a concentration of 2 and 4  $\mu\text{M}$  (IM 56), or with IM 5 or DMSO at a concentration of 10  $\mu\text{M}$ . Duplicates of the drug-conditions were co-treated with 5 mM phenformin. Samples from each condition were transferred to fix-solution and percent apoptosis was assessed as described in section 3.6. Western blotting was performed as described in section 3.8, and the membrane was incubated with antibodies for pP70S6K and P70S6K, with  $\beta$ -actin as loading control (see Table 3). The bottom graph shows amount of phosphorylated P70S6K relative to total P70S6K in treated cells relative to an untreated control. The upper graph show amount of total P70S6K. The table show percent apoptosis relative to untreated control.



Supporting Figure 2. Western blot for pAKT and AKT. MOLM-13 cells were incubated with IM 56, IM 5 and DMSO for 4 hours, at a concentration of 2 and 4  $\mu\text{M}$  (IM 56), or with IM 5 or DMSO at a concentration of 10  $\mu\text{M}$ . Duplicates of the drug-conditions were co-treated with 5 mM phenformin. Samples from each condition were transferred to fix-solution and percent apoptosis was assessed as described in section 3.6. Western blotting was performed as described in section 3.8, and the membrane was incubated with antibodies for pAKT and AKT, with  $\beta$ -actin as loading control (see Table 3). The bottom graph shows amount of phosphorylated AKT relative to total AKT in treated cells relative to an untreated control. The upper graph show amount of total AKT. The table show percent apoptosis relative to untreated control.

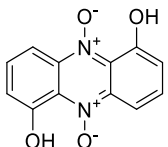
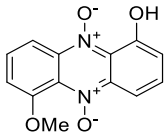
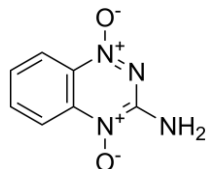
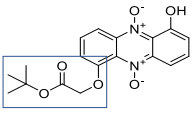
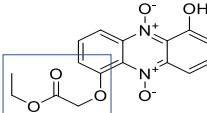
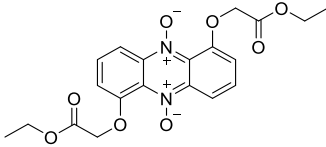
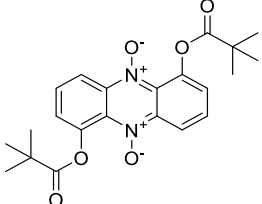


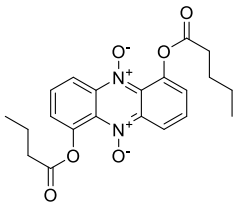
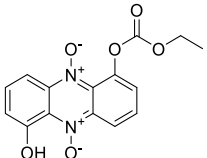
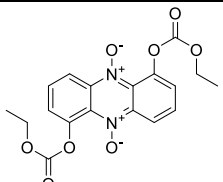
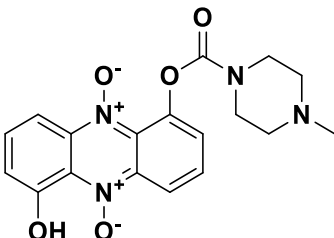
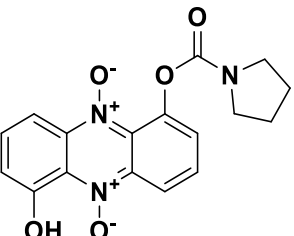
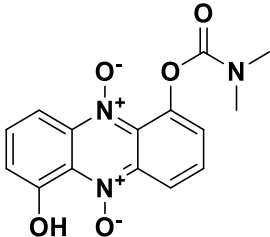
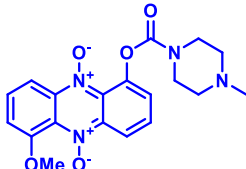
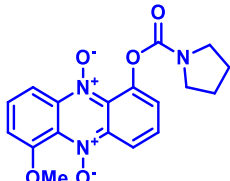
Supporting Figure 3. Example of quantification of protein expression in western blots. Performed using ImageJ Analyze>gel tool. Numbers 1-9 indicate area corresponding to the intensity of the protein band for each lane and is converted to a number. Lane for protein standard (lane 1) is not included.

## Appendix II

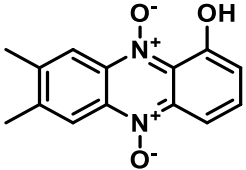
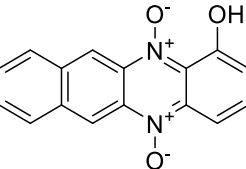
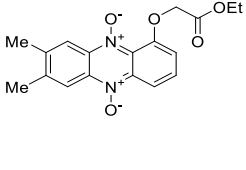
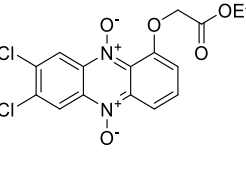
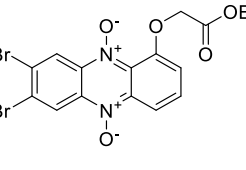
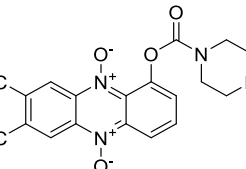
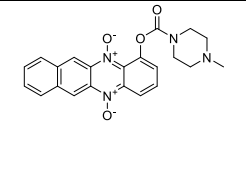
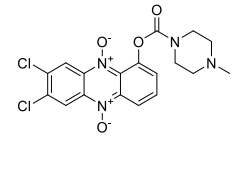
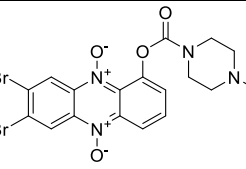
Supporting Table 1.

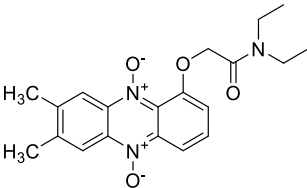
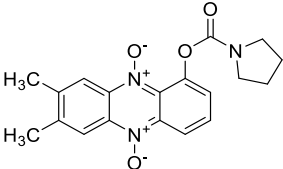
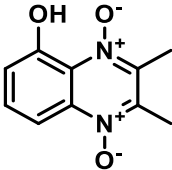
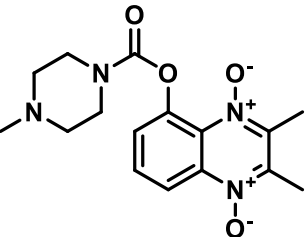
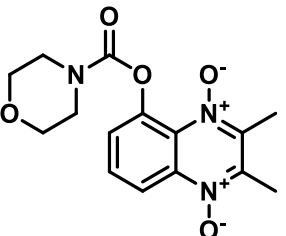
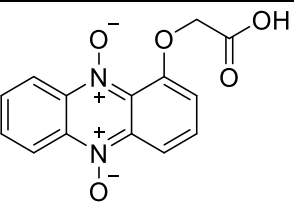
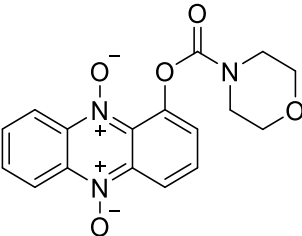
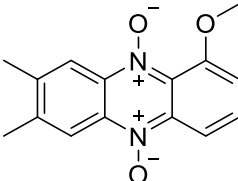
Structures and EC<sub>50</sub>-values for phenazine analogues. Table provided by Elvar Örn Viktorsson, Reidun Æsøy, Lars Herfindal and Pål Rognved. (Unpublished data).

Structure	Manus number	IM Number	Molm 13 Normox EC50 (μM)	Molm 13 Hypox EC50 (μM)	NRK Normox EC50 (μM)	NRK Hypox EC50 (μM)	H9c2 Normox EC50 (μM)
<p>Iodinin</p> 	3	IM5	2.0 ± 0.07	0.79 ± 0.10	>50 (n=3)	>50 (n=3)	>50 (n=3)
<p>Myxin</p> 	4	IM7	1.4 ± 0.30	0.77 ± 0.13	77 ± 11 (n=2)	76 ± 14 (n=2)	46 ± 4.1 (n=3)
<p>Tirapazamine</p> 	10	-	95 ± 8*	22 ± 2*	>100* (n=3)	35 ± 6.3* (n=3)	>100* (n=3)
		IM15	2.9 ± 0.34	2.4 ± 0.16	53 ± 1.5 (n=2)	53 ± 0.0 (n=2)	42 ± 5.8 (n=3)
	7	IM20	0.57 ± 0.06	0.49 ± 0.12	11 ± 1.6 (n=3)	18 ± 1.5 (n=3)	15 ± 0.9 (n=3)
		IM21	2.0 ± 0.47	0.79 ± 0.06	>20 (n=3)	>20 (n=3)	>20 (n=3)
	11	IM22	11 ± 0.7 (n=4)	8.9 ± 1.71 (n=4)	n.d.	n.d.	n.d.

Structure	Manus number	IM Number	Molm 13 Normox EC50 ( $\mu\text{M}$ )	Molm 13 Hypox EC50 ( $\mu\text{M}$ )	NRK Normox EC50 ( $\mu\text{M}$ )	NRK Hypox EC50 ( $\mu\text{M}$ )	H9c2 Normox EC50 ( $\mu\text{M}$ )
	12	IM27	$36 \pm 0.1$ (n=5)	$22 \pm 2.8$ (n=4)	n.d.	n.d.	n.d.
	13	IM23	$50 \pm 0.4$ (n=4)	$66 \pm 2.2$ (n=4)	n.d.	n.d.	n.d.
	14	IM24	$6.1 \pm 0.05$ (n=4)	$4.0 \pm 0.33$ (n=4)	>25 (n=2)	>25 (n=2)	>25 (n=2)
	15	IM32	$1.5 \pm 0.16$ (n=4)	$1.4 \pm 0.06$ (n=4)	$53 \pm 2.0$ (n=2)	$59 \pm 1.1$ (n=2)	$100 \pm 13$ (n=3)
	16	IM33	$0.86 \pm 0.047$ (n=6)	$0.79 \pm 0.089$ (n=4)	$9.6 \pm 0.38$ (n=3)	$15 \pm 1.0$ (n=3)	$12 \pm 0.7$ (n=2)
	17	IM30	$0.89 \pm 0.026$ (n=4)	$0.70 \pm 0.036$ (n=4)	$49 \pm 1.8$ (n=2)	$62 \pm 1.3$ (n=2)	$64 \pm 9.2$ (n=2)
	18	IM56	$1.0 \pm 0.06$ (n=4)	$0.98 \pm 0.081$ (n=4)	$26 \pm 2.1$ (n=3)	$39 \pm 4.2$ (n=3)	$26 \pm 0.9$ (n=3)
	19	IM58	$2.0 \pm 0.11$ (n=4)	$1.8 \pm 0.17$ (n=6)	$32 \pm 2.5$ (n=2)	$35 \pm 1.5$ (n=2)	$35 \pm 3.3$ (n=3)

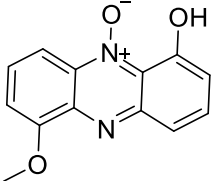
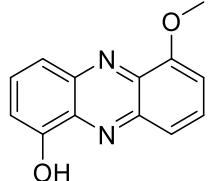
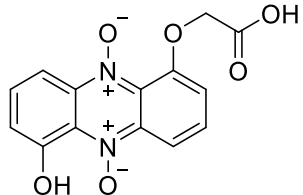
Structure	Manus number	IM Number	Molm 13 Normox EC50 ( $\mu\text{M}$ )	Molm 13 Hypox EC50 ( $\mu\text{M}$ )	NRK Normox EC50 ( $\mu\text{M}$ )	NRK Hypox EC50 ( $\mu\text{M}$ )	H9c2 Normox EC50 ( $\mu\text{M}$ )
	20	IM57	$1.9 \pm 0.07$ (n=4)	$1.7 \pm 0.09$ (n=4)	$22 \pm 1.7$ (n=2)	$29 \pm 0.7$ (n=2)	$35 \pm 1.8$ (n=3)
	21	IM35	$11 \pm 1.8$ (n=6)	$12 \pm 0.04$ (n=4)	$79 \pm 4.2$ (n=3)	>100 (n=3)	>100 (n=2)
	24	IM37	$1.5 \pm 0.14$ (n=6)	$1.7 \pm 0.29$ (n=6)	$26 \pm 0.8$ (n=3)	$25 \pm 0.2$ (n=3)	$20 \pm 2.9$ (n=2)
	25	IM40	$2.2 \pm 0.09$ (n=6)	$1.9 \pm 0.11$ (n=4)	$26 \pm 0.7$ (n=3)	$25 \pm 1.9$ (n=3)	$20 \pm 2.1$ (n=2)
	26	IM60	$1.2 \pm 0.08$ (n=4)	$1.4 \pm 0.15$ (n=6)	$13 \pm 0.01$ (n=2)	$16 \pm 1.0$ (n=2)	$23 \pm 0.1$ (n=2)
	27	IM38	$1.5 \pm 0.18$ (n=6)	$1.9 \pm 0.05$ (n=4)	$25 \pm 0.2$ (n=3)	$37 \pm 1.9$ (n=3)	$36 \pm 11$ (n=2)
	28	IM36	$1.3 \pm 0.15$ (n=6)	$2.1 \pm 0.16$ (n=4)	$19 \pm 1.3$ (n=3)	$25 \pm 0.6$ (n=3)	$16 \pm 2.6$ (n=2)
	29	IM42	$1.5 \pm 0.18$ (n=6)	$1.2 \pm 0.15$ (n=4)	$18 \pm 0.6$ (n=3)	$21 \pm 2.4$ (n=3)	$13 \pm 0.5$ (n=2)

Structure	Manus number	IM Number	Molm 13 Normox EC50 (μM)	Molm 13 Hypox EC50 (μM)	NRK Normox EC50 (μM)	NRK Hypox EC50 (μM)	H9c2 Normox EC50 (μM)
	44	IM66	2.8 ± 0.25 (n=6)	2.3 ± 0.10 (n=4)	>50 (n=2)	>50 (n=2)	>50 (n=2)
	45	IM80	Causes increased viability (n=4)	>10 (n=2)	n.d.	n.d.	n.d.
	48	IM68	8.3 ± 0.78 (n=6)	6.3 ± 0.25 (n=4)	140 ± 2 (n=2)	>100 (n=2)	>100 (n=2)
	50	IM54	0.41 ± 0.050 (n=4)	0.38 ± 0.042 (n=4)	3.1 ± 0.02 (n=2)	4.7 ± 0.09 (n=2)	1.3 ± 0.2 (n=3)
	51	IM75	2.4 ± 0.03 (n=4)	1.6 ± 0.09 (n=4)	10 ± 0.7 (n=2)	9.7 ± 2.40 (n=2)	3.3 ± 0.50 (n=2)
	52	IM69	0.63 ± 0.052 (n=6)	0.54 ± 0.060 (n=4)	11 ± 1.5 (n=3)	13 ± 0.7 (n=3)	9.4 ± 0.55
	53	IM83	2.8 ± 0.18 (n=4)	1.8 ± 0.10 (n=4)	2.0 ± 0.06 (n=2)	7.5 ± 0.38 (n=2)	2.3 ± 0.05 (n=2)
	54	IM55	0.34 ± 0.038 (n=4)	0.32 ± 0.063 (n=4)	10 ± 0.9 (n=3)	15 ± 1.8 (n=3)	3.2 ± 0.10 (n=3)
	55	IM76	0.41 ± 0.040 (n=4)	0.23 ± 0.034 (n=4)	6.2 ± 0.02 (n=2)	7.6 ± 0.60 (n=2)	2.2 ± 0.53 (n=3)

Structure	Manus number	IM Number	Molm 13 Normox EC50 ( $\mu\text{M}$ )	Molm 13 Hypox EC50 ( $\mu\text{M}$ )	NRK Normox EC50 ( $\mu\text{M}$ )	NRK Hypox EC50 ( $\mu\text{M}$ )	H9c2 Normox EC50 ( $\mu\text{M}$ )
	56	IM89	$1.8 \pm 0.24$ (n=6)	$3.4 \pm 0.78$ (n=4)	$21 \pm 0.3$ (n=2)	$52 \pm 1.2$ (n=2)	$41 \pm 5.7$ (n=2)
	57	IM88	$1.5 \pm 0.02$ (n=4)	$0.78 \pm 0.108$ (n=4)	$6.6 \pm 0.04$ (n=2)	$8.9 \pm 0.06$ (n=2)	$8.7 \pm 1.2$ (n=2)
	60	IM84	>200 (n=4)	>200 (n=4)	n.d.	n.d.	n.d.
	61	IM86	>200 (n=4)	>200 (n=4)	n.d.	n.d.	n.d.
	62	IM87	>200 (n=4)	>200 (n=4)	n.d.	n.d.	n.d.
	-	IM41	-	-	-	-	-
	-	IM61	-	-	-	-	-
	-	IM62	-	-	-	-	-



Supporting Table 2.

Supporting Table 2. Structures and EC <sub>50</sub> -values of phenazine analogues not provided in Supporting Table 1. Data from Viktorsson et al (2017, Table 1).				
Structure	Name	Cpd no.:	IC <sub>50</sub> [μM]	
			Normoxia	Hypoxia
	IM11	12	147 ± 17*	22 ± 9.1
	IM2	14	276 ± 17	39 ± 16
	IM18	19	54 ± 13	61 ± 8